PHLDA3 may have a tumor suppressive function (8). However, there has hitherto been no reported role for PHLDA3 in human tumors, and its in vivo function has remained elusive. In this report, we demonstrate that the *PHLDA3* gene is a novel tumor suppressor, inactivation of which can lead to the development of PanNETs. We show that the *PHLDA3* genomic locus undergoes LOH and that the *PHLDA3* promoter is methylated at a high frequency in PanNETs. Furthermore, analysis of *PHLDA3*-deficient mice showed that these mice frequently develop islet hyperplasia as a result of enhanced islet cell proliferation and an increase in islet cell size. Collectively, these results indicate that PHLDA3 functions as a tumor suppressor in PanNETs.

## Results

**Frequent LOH at the *PHLDA3* Gene Locus in PanNETs.** The *PHLDA3* gene is located at 1q31, a locus that has been reported to have a high frequency of LOH in two NETs derived from pancreas: insulinomas and gastrinomas (9, 10). We therefore speculated that the *PHLDA3* locus may undergo LOH in PanNETs, and analyzed the *PHLDA3* locus for LOH using microsatellite markers surrounding the gene in 54 PanNET samples (Fig. 1 *A–D*; clinical diagnosis for each sample is shown in *SI Appendix*, Fig. S1*A*). As shown in Fig. 1*B*, out of 54 PanNETs, 50 samples were informative and 36 samples showed LOH at the *PHLDA3* locus. The incidence of LOH at the *PHLDA3* locus (72%) is remarkably high, and was comparable to the reported LOH incidence of the *Multiple endocrine neoplasia type 1 (MEN1)* gene, which has the highest reported incidence of genomic changes in PanNETs (11). Within the region analyzed, the LOH frequency peaks near the *PHLDA3* locus, suggesting that LOH of the *PHLDA3* gene is critical for PanNET development (Fig. 1*D*). This tendency becomes clearer when samples that exhibit partial LOH within this region (PanNET 1–18) were analyzed (Fig. 1*D*, blue line). A strikingly high incidence of LOH at the *PHLDA3* locus indicates the importance of this PHLDA3-regulated tumor suppression pathway in PanNETs. Most of the PanNETs analyzed in this study are nonfunctional, and we found no associations between *PHLDA3* LOH and specific PanNET type or insulin/glucagon positivity, to the extent that we examined this (*SI Appendix*, Fig. S1).

**PHLDA3 and MEN1 Cooperatively Suppress PanNET.** The most outstanding genomic aberration previously reported in PanNETs was the mutation and LOH of the *MEN1* gene, a tumor suppressor gene associated with multiple endocrine neoplasia type 1

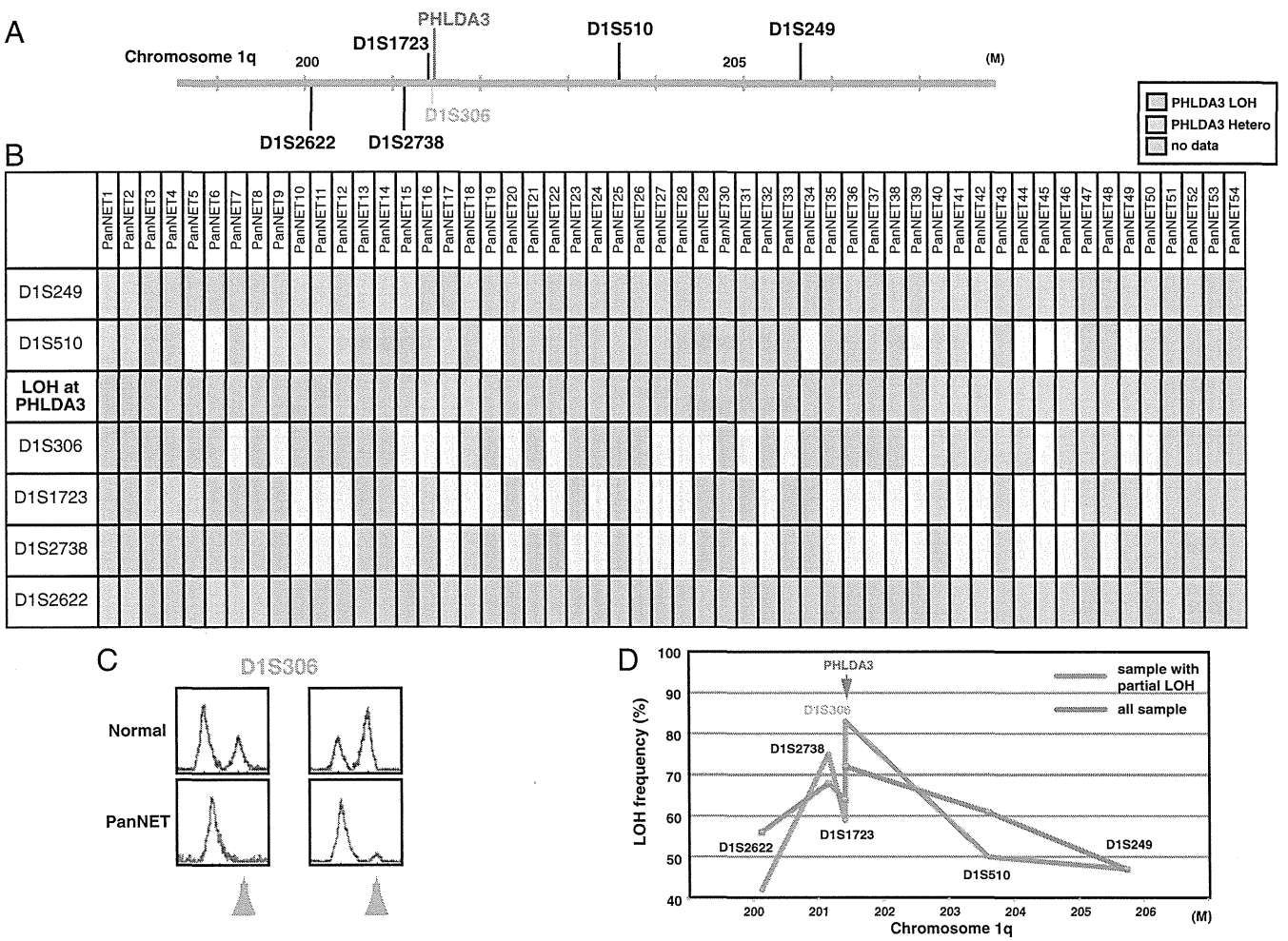


**Fig. 1.** Frequency of LOH at the *PHLDA3* gene locus in PanNETs. (*A*) Chromosomal locations of *PHLDA3* gene and microsatellite markers used in this study. D1S306 is located just next to the *PHLDA3* gene (32 kb upstream). (*B*) Microsatellite analysis of the *PHLDA3* gene locus region. PanNET samples were analyzed for LOH around the *PHLDA3* gene locus. Because D1S306 is located next to the *PHLDA3* gene, the LOH status of the *PHLDA3* gene was determined from the LOH status of the D1S306 locus. For some loci with no data (not informative or data unavailable), the LOH status of the locus was determined from the surrounding LOH status (shown in faint pink and faint blue). (*C*) Representative microsatellite analysis results. In normal tissues, two peaks derived from maternal and paternal alleles were detected, whereas in tumors, one allele was lost (shown by orange arrows), indicating LOH at the locus. (*D*) LOH frequency for each microsatellite marker. Frequencies from all samples (shown by red line) and frequencies from samples showing LOH partially within the analyzed region (PanNET1-18, shown by blue line) are shown.

(7, 11). It has been reported that ~50% of PanNET cases exhibit LOH of the *MEN1* gene. Therefore, we analyzed whether *MEN1* LOH is observed in our PanNET samples. As shown in Fig. 2 *A* and *B*, 32 samples out of 48 informative samples showed LOH at the *MEN1* locus. Frequent LOH was observed at the *MEN1* locus in our samples (67%), confirming previous studies. We next combined the LOH data for the *PHLDA3* and *MEN1* loci. As shown in Fig. 2*C*, LOH at the *PHLDA3* and *MEN1* loci did not show a mutually exclusive pattern, which would be expected if PHLDA3 and MEN1 were on the same tumor suppressing pathway. Interestingly, we observed a significant frequency of double LOH, i.e., occurring at both the *PHLDA3* and *MEN1* loci (25 of 45 samples, $P < 0.05$ by Fisher's exact test). These data suggest that development of PanNET involves the functional loss of both pathways.

**LOH at the *PHLDA3* Locus Is Correlated to Poor Prognosis in PanNET Patients.** To select the proper treatment for each PanNET patient, prediction of disease prognosis is important. We observed that LOH at the *PHLDA3* locus was associated with advanced stage PanNETs, whereas absence of LOH was associated with lower tumor grades. These associations were statistically significant ($P < 0.01$, by Fisher's exact test), suggesting that the LOH is associated with a malignant phenotype in PanNETs (Fig. 3*A*). We next analyzed the relationship between LOH at the *PHLDA3* locus and the prognosis of PanNET patients. As shown in Fig. 3*B*, patients exhibiting LOH at the *PHLDA3* locus seemed to have a poorer prognosis compared with the patients without LOH. However, the observed difference did not achieve statistical significance, probably due to the relatively small numbers of patients analyzed. On the other hand, LOH at the *MEN1* locus had no influence on tumor grade or patient survival, as has been reported (7) (Fig. 3 *C* and *D*). It will be necessary to extend these studies with larger numbers of patients before reaching a firm conclusion, however these results suggest that the PHLDA3-regulated pathway, but not the MEN1-regulated pathway, may be a critical determinant of the prognosis of PanNET patients.

**The *PHLDA3* Gene Undergoes Aberrant Methylation in Addition to LOH in PanNETs.** Because we found frequent LOH at the *PHLDA3* locus in PanNETs, we next examined how the remaining allele is inactivated. The *PHLDA3* gene is mutated in several cancers: 11 mutations in lung, urinary, and large intestine cancer are reported in the COSMIC database (http://cancer.sanger.ac.uk/cancergenome/projects/cosmic), and mutation in lung cancer was reported by Yoo et al. (12). Therefore, we analyzed the *PHLDA3* ORF genomic sequence in our PanNET samples, but did not find any mutations within the coding regions (*SI Appendix*, Fig. S2). We next analyzed *PHLDA3* mRNA expression levels in these PanNETs. As shown in Fig. 4*A*, *PHLDA3* expression was significantly lower in samples showing LOH at the *PHLDA3* locus compared with samples without LOH. We noticed a CpG island overlapping the promoter region and the first exon of the *PHLDA3* gene (Fig. 4*B*). We therefore analyzed whether the methylation status of the *PHLDA3* gene is related to *PHLDA3* transcription levels. Specifically, we analyzed DNA methylation levels within the first exon of the *PHLDA3* gene, because it has been reported that methylation of the first exon is tightly linked to transcriptional silencing (13). Analysis of *PHLDA3* mRNA expression levels in four cancer cell lines revealed that *PHLDA3* is highly expressed in LNCaP and MDA-MB-M468 cells, whereas expression is very low in DLD1 and H1299 cells (Fig. 4*C*). Analysis of DNA methylation levels by methylation-specific PCR revealed detectable methylation only in DLD1 and H1299 cells, cell lines with low *PHLDA3* expression (Fig. 4*D*). It is of note that, in H1299 cells, a human lung NET cell line, *PHLDA3* mRNA expression was remarkably low and methylation was remarkably high. We further treated H1299 cells with 5-aza-C to demethylate the *PHLDA3* gene. As shown in Fig. 4*E*, 5-aza-C treatment resulted in decreased methylation at the *PHLDA3* gene and

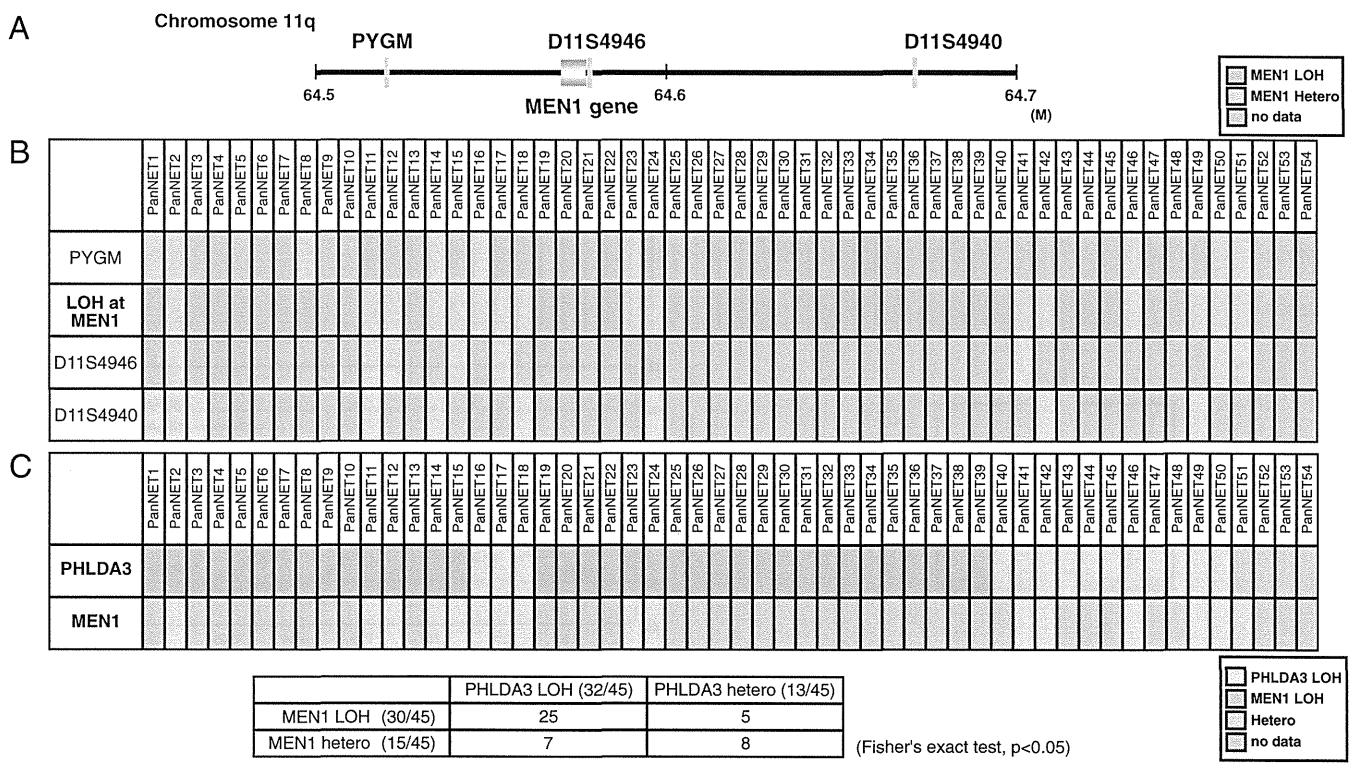


| | PHLDA3 LOH (32/45) | PHLDA3 hetero (13/45) |
|---|---|---|
| MEN1 LOH (30/45) | 25 | 5 |
| MEN1 hetero (15/45) | 7 | 8 |

(Fisher's exact test, p<0.05)

**Fig. 2.** Relationship between PHLDA3 and MEN1 tumor-suppressing pathways. (*A*) Chromosomal locations of the *MEN1* gene and microsatellite markers used in this study. (*B*) Analysis of LOH at the *MEN1* locus. The LOH status of the *MEN1* gene was determined from the LOH status of either of the informative markers. (*C*) Relationship between LOH status of the *PHLDA3* and *MEN1* loci. In total, 45 samples informative for both *PHLDA3* and *MEN1* loci were analyzed.

A

| | grade 1or 2 | grade 3 or 4 |
|---|---|---|
| PHLDA3 LOH + | 10 | 21 |
| PHLDA3 LOH- | 11 | 3 |

(p<0.01, Fisher's exact test)

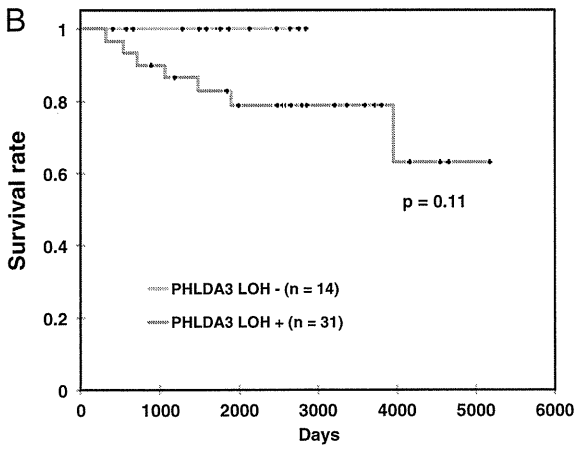


C

| | grade 1or 2 | grade 3 or 4 |
|---|---|---|
| MEN1 LOH + | 19 | 19 |
| MEN1 LOH- | 4 | 3 |

(p=0.73, Fisher's exact test)

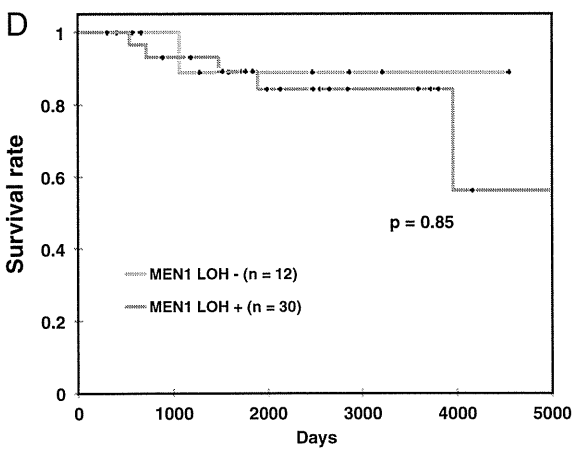


**Fig. 3.** LOH at the *PHLDA3* and *MEN1* gene locus and progression of PanNETs. (*A*) LOH at the *PHLDA3* gene locus and grade of PanNETs. The *P* value was calculated by Fisher's exact test. (*B*) Kaplan–Meier plots of overall survival of patients with PanNETs. Fourteen or 31 patients without or with *PHLDA3* LOH were analyzed. Wilcoxon test was used to determine the *P* value. (*C*) LOH at the *MEN1* gene locus and grade of PanNETs. (*D*) Kaplan–Meier plot for overall survival of patients with PanNETs. Twelve or 30 patients without or with *MEN1* LOH were analyzed as in *B*.

enhanced expression of *PHLDA3* in a 5-aza-C concentration-dependent manner. A similar result was obtained using a human PanNET cell line A99 (Fig. 4*F*) and the mouse insulinoma cell line MIN6 that has very low PHLDA3 expression (*SI Appendix*, Fig. S3 *A* and *B*). These results indicate that methylation of the *PHLDA3* gene affects *PHLDA3* transcription levels. We then analyzed the methylation status of the *PHLDA3* promoter in PanNET samples that had undergone LOH at the *PHLDA3* locus. As shown in Fig. 4*G*, methylation was not detected in normal pancreas or islets, whereas significant methylation was detected in all LOH+ samples (seven of seven) analyzed. These results show that the *PHLDA3* gene can undergo methylation in addition to LOH in PanNETs, indicating that a two-hit inactivation of the *PHLDA3* gene may often occur. We also analyzed LOH– samples and found detectable levels of methylation in two of four samples (*SI Appendix*, Fig. S4). Thus, the repression of *PHLDA3* expression in LOH– samples due to methylation may also contribute to tumor progression in PanNETs.

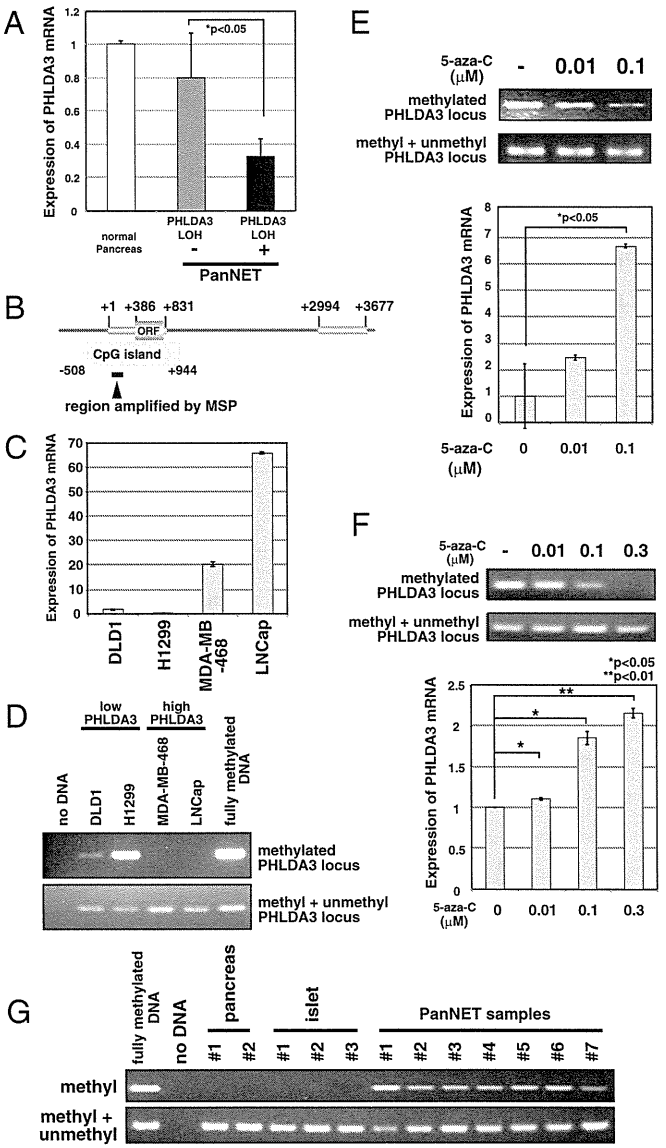


**Fig. 4.** *PHLDA3* expression and promoter region methylation status in PanNETs. (*A*) *PHLDA3* gene expression in PanNETs. Total RNAs were prepared from normal pancreas and PanNETs. RNA was pooled from 5 normal pancreases for the normal controls. RNA was isolated from PanNET samples with (10 samples) or without LOH (7 samples). Gene expression was quantitated by RT-PCR and normalized to *GAPDH*. (*B*) Genomic organization of *PHLDA3* promoter region and location of CpG island. Wide lines indicate exonic regions of the *PHLDA3* gene (+1 to +831 and +2994 to +3677). (*C*) *PHLDA3* gene expression in cell lines. Gene expression was analyzed as in *A*. (*D*) DNA methylation of the *PHLDA3* promoter. Genomic DNAs from the indicated cell lines were analyzed by methylation-specific PCR. Positions of the primers used in the assay are shown in *B*. Primers designed to amplify methylated DNA (upper panel) or DNA with or without DNA methylation (lower panel) were used. Fully methylated DNA was used as a control. (*E* and *F*) 5-aza-C treatment of Lung NET H1299 cells (*E*) or PanNET A99 cells (*F*). Both genomic DNAs and total RNAs were isolated, and analyzed as in *D* and *A*, respectively. (*G*) Methylation status of *PHLDA3* promoter in normal pancreas, normal isolated islets and PanNETs (samples showing LOH at the *PHLDA3* locus was analyzed). Genomic DNAs were prepared and analyzed as in *D*.

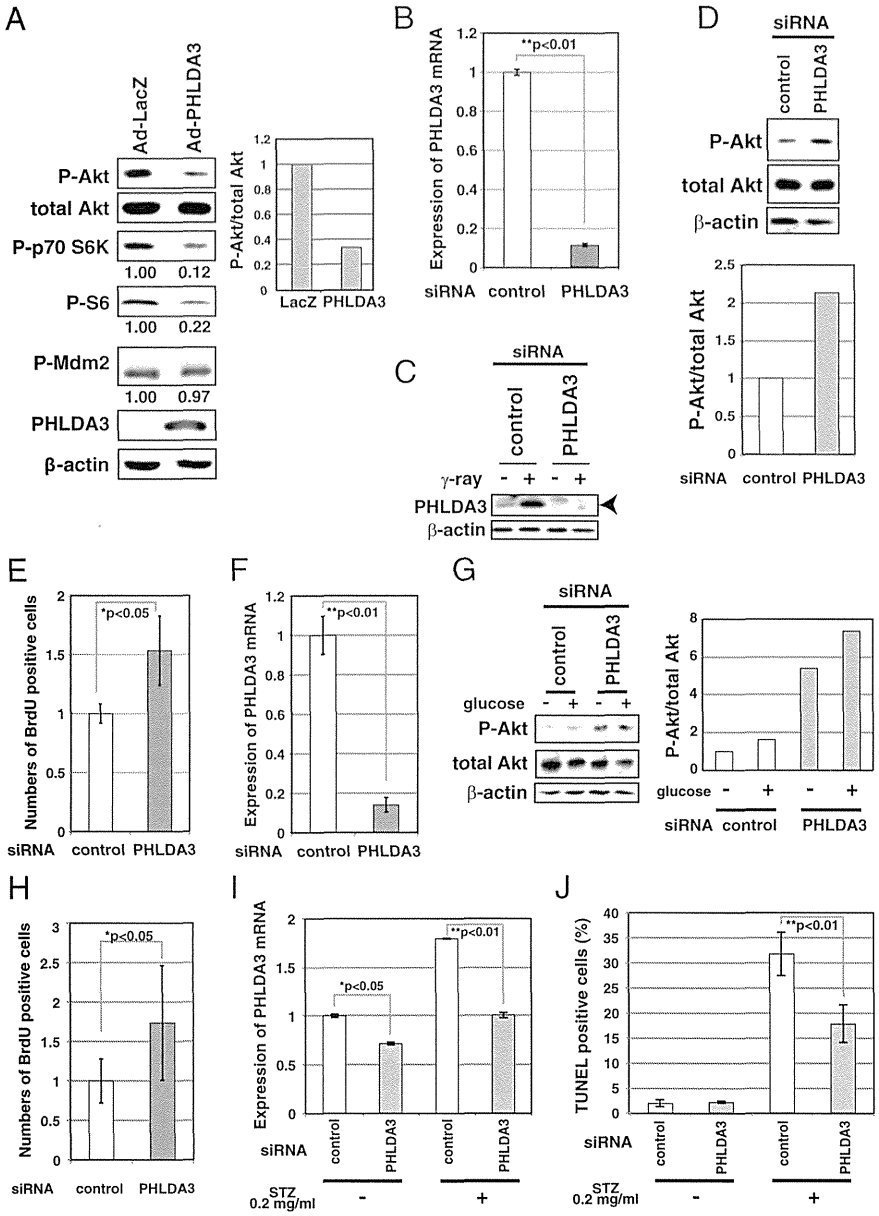


Fig. 5. Effect of PHLDA3 expression on Akt activity, cell proliferation and apoptosis of islet cells. (*A*) Effect of PHLDA3 expression on Akt activity in MIN6 cells. MIN6 cells were transduced with Ad-LacZ or Ad-PHLDA3 at a moi of 35, and harvested 30 h post-infection. Akt activation and phosphorylation of Akt downstream signaling molecules were analyzed by Western blotting and quantified by normalization to total Akt levels (P-Akt) or by β-actin levels (P-p70 S6K, P-S6, P-Mdm2). (*B* and *C*) Efficiency of siRNA inhibition of PHLDA3 expression in RIN cells. RIN cells were transfected with control or PHLDA3 siRNAs. *PHLDA3* mRNA levels were analyzed 31 h posttransfection by quantitative RT-PCR, standardized against β-actin (*B*). PHLDA3 protein levels were also determined 48 h posttransfection by Western blotting (*C*), using cells subjected to γ-ray irradiation (20 Gy) versus untreated. The γ-ray irradiated samples were included to help identify the band representing PHLDA3 protein (PHLDA3 is induced by p53 activation). (*D*) Effect of PHLDA3 expression on Akt activation in RIN cells. RIN cells were transfected as in *B* and Akt activation was analyzed by Western blotting 31 h posttransfection (left) and quantified by normalization to total Akt levels (right). (*E*) Effect of PHLDA3 expression on RIN cell proliferation. RIN cells were transfected as in *B*, and labeled with BrdU for 3 h and harvested 28 h post transfection. BrdU positive cells were quantified by using Ziva Ultrasensitive BrdU assay. (*F*) siRNA suppression of *PHLDA3* expression in primary islet cells. Isolated primary islet cells were transfected with control or PHLDA3 siRNA, harvested 30 h post transfection, and *PHLDA3* mRNA levels were analyzed by quantitative RT-PCR as in *B*. (*G*) Effect of PHLDA3 expression on Akt activation in primary islet cells. Cells were transfected with siRNA as in *F* and 48 h post-transfection were treated with glucose (30 mM) for 20 min. Levels of Akt activation were analyzed as in *D*. (*H*) Effect of PHLDA3 expression on primary islet cell proliferation. Cells were transfected as in *F*, labeled with BrdU for 4 h and harvested 30 h post transfection. BrdU positive cells were analyzed as in *E*. (*I* and *J*) Effect of PHLDA3 expression on STZ-induced apoptosis of primary rat islets. Isolated islets were pooled from three rats, and transfected with control or PHLDA3 siRNA. At 75 h posttransfection, islets were treated with STZ (20 μg/mL) for 30 min. Islets were then cultured overnight, and total RNAs were prepared and *PHLDA3* expression was analyzed by quantitative RT-PCR as in B (*I*), or subjected to TUNEL staining and analyzed by FACS (*J*).

**PHLDA3 Controls Akt Activity, Cell Proliferation, and Apoptosis of Islet Cells.** PanNETs are derived from pancreatic islet endocrine cells. It is well known that, in islet β cells, Akt signaling plays a central role in promoting cell growth and inhibiting apoptosis (5). Therefore, in β cells, loss of PHLDA3 function may result in the hyperactivation of Akt oncogenic signaling, and thus lead to tumor progression. To analyze the function of PHLDA3 in islet β cells, we examined RIN and MIN6 cells, cell lines derived from pancreatic β cells (Fig. 5 *A–E*). Whereas RIN cells have detectable levels of PHLDA3 expression, MIN6 has very low PHLDA3 expression (*SI Appendix*, Fig. S3*A*). We first used a gain-of-function approach to confirm that PHLDA3 functions as a repressor of Akt in MIN6 cells. As shown in Fig. 5*A*, expression of PHLDA3 resulted in decreased Akt activation levels and decreased phosphorylation of signaling molecules downstream of Akt. Similar results were obtained using *PHLDA3*$^{-/-}$ mouse embryonic fibroblasts (MEFs, *SI Appendix*, Fig. S5). Next, we knocked down PHLDA3 expression in RIN cells using siRNA against PHLDA3 (Fig. 5 *B* and *C*), and observed increased Akt activation and cell proliferation (Fig. 5 *D* and *E*). We observed similar results in normal primary rat islet cells, i.e., knockdown of PHLDA3 expression resulted in activation of Akt (with or without glucose stimulation) and significant enhancement of cell proliferation (Fig. 5 *F–H* and *SI Appendix*, Fig. S6). Next, we analyzed the effect of PHLDA3 expression on the apoptosis of islet cells induced by Streptozotocin (STZ), a chemical that is particularly toxic to insulin-producing β cells (14). We observed that although inhibition of *PHLDA3* expression by siRNA was relatively poor in isolated rat islets (Fig. 5*I*), this knockdown significantly reduced the number of apoptotic cells caused by STZ treatment (Fig. 5*J*). Collectively, these results demonstrate that PHLDA3 controls Akt activity, cell growth, and the apoptosis of islet cells.

**Development of Hyperplastic Islets in *PHLDA3*-Deficient Mice.** To analyze the effect of PHLDA3 deficiency on islets in vivo, we examined the pancreases of *PHLDA3*-deficient mice. Differences in islet sizes were not detected in 3-mo-old *PHLDA3*$^{+/+}$ or *PHLDA3*$^{-/-}$ mice (*SI Appendix*, Fig. S7). However, in 6-mo-old *PHLDA3*$^{-/-}$ mice, we found significantly fewer islets that were smaller than 0.01 mm$^2$ and significantly more islets that were larger than 0.01 mm$^2$, compared with *PHLDA3*$^{+/+}$ mice (Fig. 6 *A* and *C*).

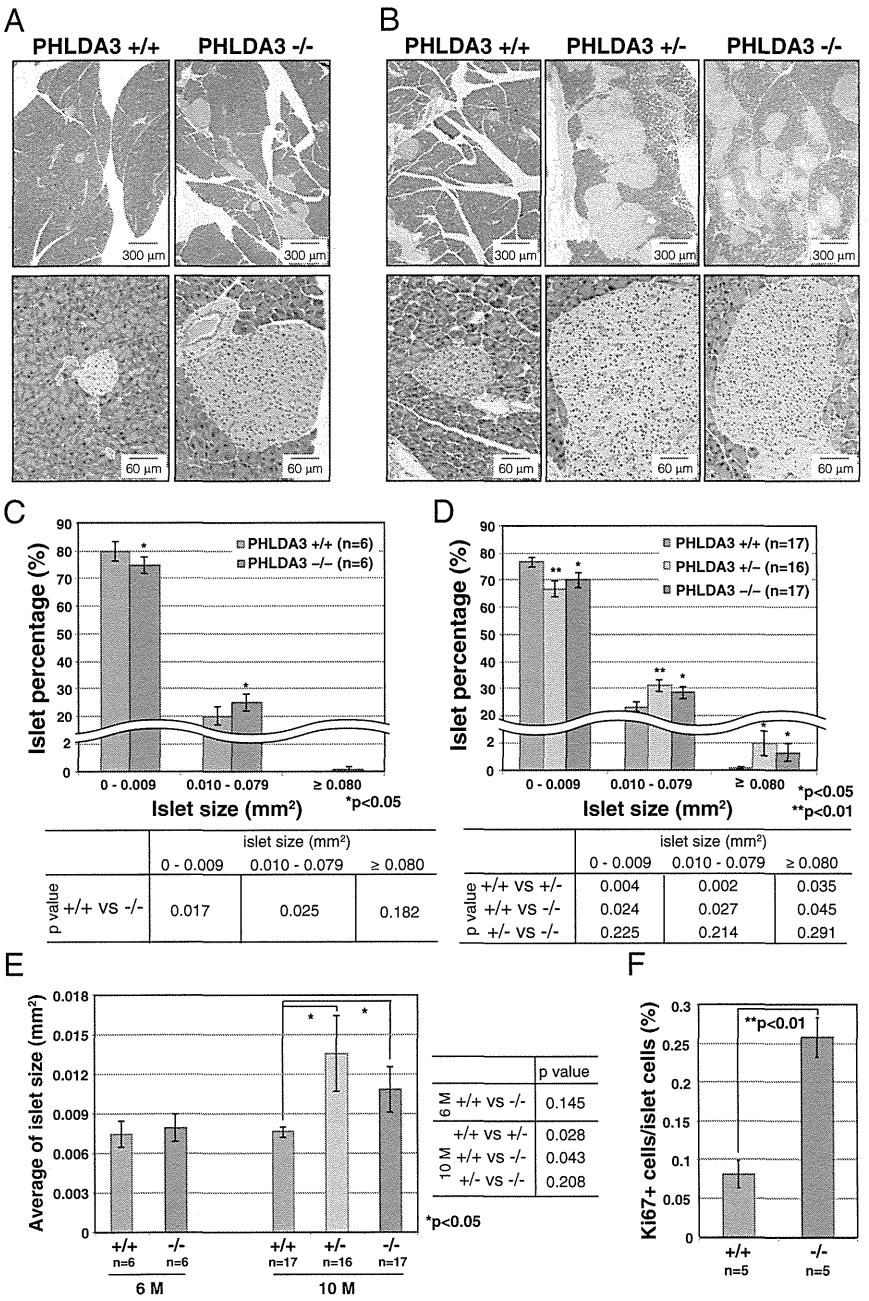


| | islet size (mm²) | | |
|---|---|---|---|
| | 0 - 0.009 | 0.010 - 0.079 | ≥ 0.080 |
| p value +/+ vs -/- | 0.017 | 0.025 | 0.182 |

| | islet size (mm²) | | |
|---|---|---|---|
| | 0 - 0.009 | 0.010 - 0.079 | ≥ 0.080 |
| p value +/+ vs +/- | 0.004 | 0.002 | 0.035 |
| +/+ vs -/- | 0.024 | 0.027 | 0.045 |
| +/- vs -/- | 0.225 | 0.214 | 0.291 |

| | | p value |
|---|---|---|
| 6 M | +/+ vs -/- | 0.145 |
| 10 M | +/+ vs +/- | 0.028 |
| | +/+ vs -/- | 0.043 |
| | +/- vs -/- | 0.208 |

**Fig. 6.** Hyperplastic islets in *PHLDA3*-deficient mice. Six-month-old (21- to 31-wk-old) (*A*, *C*, and *E*) and 10-mo-old (39- to 49-wk-old) (*B* and *D–F*) mice were analyzed. (*A* and *B*) Hematoxylin and eosin staining of islets from wild-type, heterozygote and *PHLDA3*-deficient mice (*A*, 6-mo; *B*, 10-mo). (*C–E*) Calculation of islet sizes. Islet areas were calculated from hematoxylin and eosin-stained pancreas sections. One (6-mo-old mice) or three pancreas sections (10-mo-old mice; sections separated by more than 20 μm *z* axis) were analyzed per mouse. Islet areas from indicated numbers (n) of mice were analyzed. Size distributions of islets (*C*, 6-mo; *D*, 10-mo) and average islet sizes (*E*; 6- and 10-mo-old) are shown. The *P* values between $PHLDA3^{+/+}$ and $PHLDA3^{+/-}$ or $PHLDA3^{-/-}$ were calculated and are shown (*$P < 0.05$; **$P < 0.01$). (*F*) Quantitation of Ki67-positive cells. Pancreas sections from indicated numbers (n) of mice were analyzed. Islet nuclei number and Ki67-positive nuclei number were counted and the percentage of Ki67-positive cells was calculated. (**$P < 0.01$) Representative images are shown in *SI Appendix*, Fig. S4.

However, the overall average islet size at 6 mo was not significantly different between $PHLDA3^{+/+}$ and $PHLDA3^{-/-}$ mice (Fig. 6*E*). At 10 mo, abnormally large islets (larger than 0.08 $mm^2$) were frequently found (Fig. 6 *B* and *D*), and the average islet sizes were significantly larger in 10-mo-old $PHLDA3^{+/-}$ and $PHLDA3^{-/-}$ mice compared with $PHLDA3^{+/+}$ mice (Fig. 6*E*). Thus, a difference in islet sizes between $PHLDA3^{+/+}$ and $PHLDA3^{-/-}$ mice appears to emerge between 3 and 10 mo of age. We stained the islets with Ki67 antibody and found significantly more Ki67-positive cells in $PHLDA3^{-/-}$ islets compared with the $PHLDA3^{+/+}$ islets (Fig. 6*F*; representative images are shown in *SI Appendix*, Fig. S8). These data show that loss of PHLDA3 expression results in enhanced proliferation of islet cells.

**Enhanced Proliferation of β Cells and Altered Glucose Metabolism in *PHLDA3*-Deficient Mice.** The islets were further stained with anti-insulin and anti-glucagon antibodies to determine the numbers of β and α cells, respectively, within the islets. Normal murine islets have β cells in the center of the islet and α cells at the periphery surrounding the β cells (as shown in $PHLDA3^{+/+}$ islets in Fig. 7*A*). However, in the hyperplastic islets of $PHLDA3^{+/-}$ and $PHLDA3^{-/-}$ mice, huge numbers of β cells and relatively small numbers of α cells were often observed, and the hyperplastic islets often showed abnormal islet architecture, with few α cells at the periphery of the islets (Fig. 7*A*). We calculated the areas occupied by α and β cell types to determine which of these had increased. As shown in Fig. 7*B*, the mean percentage area occupied by β cells was significantly higher in $PHLDA3^{-/-}$ islets. The area occupied by β cells was also significantly high in large $PHLDA3^{-/-}$ islets (larger than 0.05 $mm^2$) compared with that seen in large islets infrequently found in $PHLDA3^{+/+}$ mice (Fig. 7*B*). Because we had found a significantly higher number of proliferating cells in $PHLDA3^{-/-}$ islets (Fig. 6*F*), we stained the islets with anti-Ki67, -insulin, and -glucagon antibodies to identify which cell types within the islets were proliferating. As shown in Fig. 7*C*, we found that most Ki67-

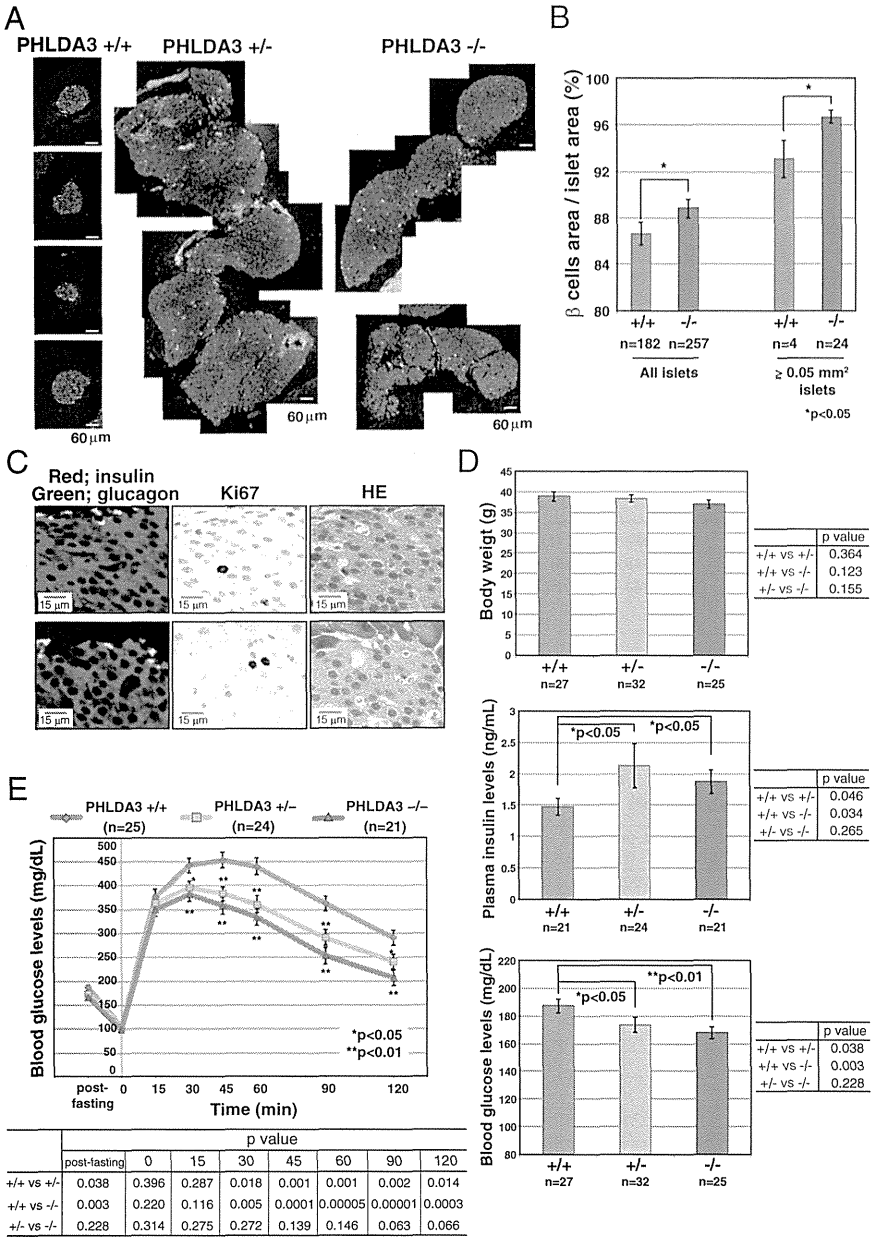


**Fig. 7.** Proliferation of β cells in the islets of *PHLDA3*-deficient mice. Ten-mo-old (39- to 49-wk-old) mice were analyzed. (*A*) Distribution of β and α cells in pancreas sections. Pancreas sections were stained with antibodies to identify β cells (anti-insulin; red) and α cells (anti-glucagon; green). Representative images of hyperplastic islets from *PHLDA3*$^{+/-}$ and *PHLDA3*$^{-/-}$ mice are shown. (*B*) Percent area occupied by β cells. Pancreas sections were stained as in *A*, and areas occupied by α- and β-cells in indicated numbers of islets from *PHLDA3*$^{+/+}$ (five mice were analyzed) and *PHLDA3*$^{-/-}$ (six mice were analyzed) were calculated and percentages of β-cell areas in the islets were determined. Semihyperplasic islets and hyperplastic islets (larger than 0.05 mm$^2$ islet area) were separately calculated and shown at the right. (*$P < 0.05$; **$P < 0.01$). (*C*) Proliferation in pancreas sections. Serial pancreas sections of *PHLDA3*$^{-/-}$ mice were stained with anti-insulin and anti-glucagon, anti-Ki67 and HE, to determine the cell types that are Ki67 positive. Representative images are shown. (*D*) Body weight, blood glucose and insulin levels. Indicated numbers (n) of mice were analyzed. Plasma insulin levels and blood glucose levels were determined in blood from tail vein samples, and were determined twice for each mouse. Mice were fed ad libitum. (*$P < 0.05$; **$P < 0.01$). (*E*) Glucose tolerance test (GTT). Indicated numbers (n) of overnight-fasted mice were subjected to GTT by i.p. injection of glucose (2 mg/g body weight). GTT was performed twice for each mouse. The *P* values between *PHLDA3*$^{+/+}$ and *PHLDA3*$^{+/-}$ or *PHLDA3*$^{-/-}$ were calculated and are shown in the panels (*$P < 0.05$; **$P < 0.01$). The differences between *PHLDA3*$^{+/-}$ and *PHLDA3*$^{-/-}$ were not significant ($P > 0.05$).

positive cells were β cells in *PHLDA3*$^{-/-}$ islets. Taken together, these data show that islet β cell proliferation is enhanced in *PHLDA3*-deficient islets.

It would be expected that abnormal proliferation of β cells would result in the excess production of insulin, leading to altered glucose metabolism in *PHLDA3*-deficient mice. As shown in Fig. 7*D*, although the *PHLDA3* genotype had no influence on body weights, 10-mo-old *PHLDA3*$^{+/-}$ and *PHLDA3*$^{-/-}$ mice had higher plasma insulin and lower blood glucose levels compared with age-matched wild-type mice under fed conditions. Similar results were obtained in 6-mo-old fed mice (*SI Appendix*, Fig. S9*A*) and in 10-mo-old fasted mice (*SI Appendix*, Fig. S9*B*). Therefore, we performed glucose tolerance tests and found significant enhancement of glucose tolerance in *PHLDA3*$^{+/-}$ and *PHLDA3*$^{-/-}$ mice (Fig. 7*E*). These data show that loss of PHLDA3 expression results in enhanced proliferation of islet cells, especially β cells, and consequential increase of insulin secretion.

We further characterized *PHLDA3*$^{-/-}$ islets using several β cell markers: the endocrine cell marker chromogranin A (*SI Appendix*, Fig. S10), the β cell differentiation marker Glut2 (*SI Appendix*, Fig. S11), and deposition of IAPP (islet amyloid polypeptide; *SI Appendix*, Fig. S12). None of these markers showed significant difference compared with *PHLDA3*$^{+/+}$ islets, indicating that *PHLDA3*$^{-/-}$ islets retain normal β cell characteristics, to the extent we examined.

***PHLDA3*-Deficient Islets Have Enhanced Akt Activity and Larger Cell Size, and Are Resistant to Apoptosis.** We further analyzed the effects of PHLDA3 deficiency on several Akt-regulated biological processes. We first confirmed reduction or loss of *PHLDA3* expression in *PHLDA3*$^{+/-}$ and *PHLDA3*$^{-/-}$ mice islets (Fig. 8*A*). We found that activation of Akt and phosphorylation of its downstream molecules were augmented in *PHLDA3*$^{-/-}$ islets (Fig. 8*B*). It has been reported that enhanced Akt activity has an effect on islet cell size (5, 6). We therefore analyzed islet cell size in *PHLDA3*$^{+/+}$, *PHLDA3*$^{+/-}$, and *PHLDA3*$^{-/-}$ mice. As shown in Fig. 8*C*, islet cell size was significantly increased in *PHLDA3*$^{-/-}$ and *PHLDA3*$^{+/-}$ mice. We next analyzed the sensitivity of *PHLDA3*$^{-/-}$ islets to apoptosis. Wild-type or *PHLDA3*$^{-/-}$ mice were treated with STZ for 5 consecutive days to produce β cell injury. It is known that STZ-induced apoptosis of β

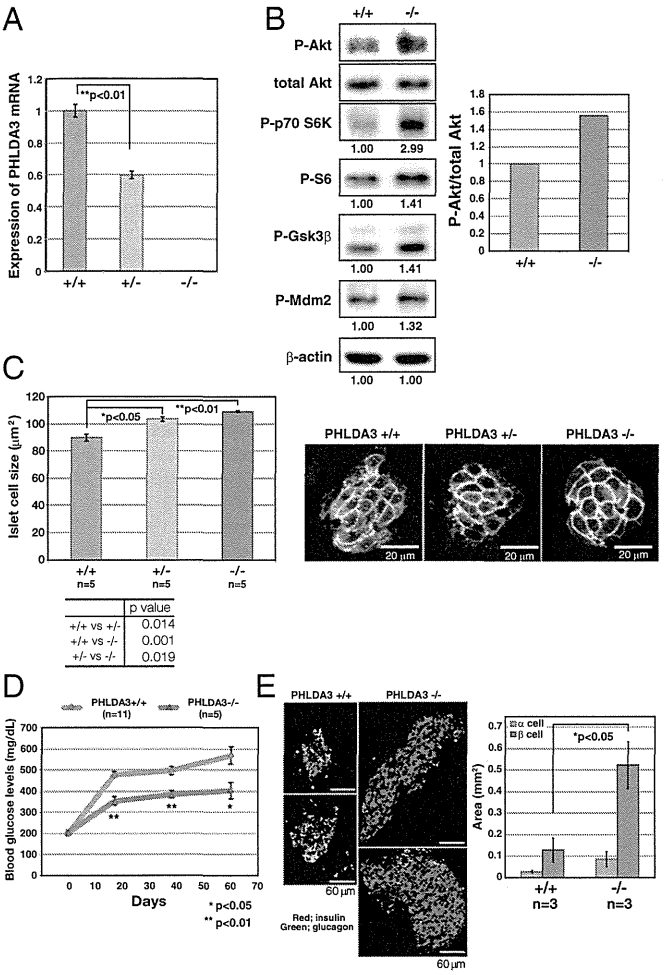


**Fig. 8.** Akt activation in islets of *PHLDA3*-deficient mice. (*A*) *PHLDA3* mRNA expression in isolated islets. Islets were isolated from $PHLDA3^{+/+}$, $PHLDA3^{+/-}$, and $PHLDA3^{-/-}$ mice, and analyzed for *PHLDA3* expression by quantitative RT-PCR, normalized to β-actin. (*B*) Akt activity and phosphorylation of Akt downstream signaling molecules in isolated islets. Akt activation and phosphorylation of Akt downstream signaling molecules were analyzed by Western blotting and quantified by normalization to total Akt levels (P-Akt, *Right*) or by β-actin levels (P-p70 S6K, P-S6, P-GSK3β, and P-Mdm2). (*C*) Islet cell size in *PHLDA3*-deficient mice. (*Left*) Indirect immunofluorescence staining of Glut2 in pancreas section from 10-mo-old mice. (*Right*) Islet areas and nuclei numbers were calculated, and mean islet cell sizes were determined from one hematoxylin- and eosin-stained pancreas sections per indicated numbers (n) of mice. The *P* values between $PHLDA3^{+/+}$ and $PHLDA3^{+/-}$ or $PHLDA3^{-/-}$ were calculated and shown in the panels (*$P < 0.05$; **$P < 0.01$). The difference between $PHLDA3^{+/-}$ and $PHLDA3^{-/-}$ was also significant ($P < 0.05$). (*D*) Blood glucose levels in streptozotocin-induced diabetic mice. Indicated numbers (n) of $PHLDA3^{+/+}$ or $PHLDA3^{-/-}$ mice were injected i.p. with STZ for 5 consecutive days. Blood glucose levels were determined at different time points as indicated after administration of STZ. (*$P < 0.05$; **$P < 0.01$). (*E*) Distribution of β and α cells in STZ-treated $PHLDA3^{+/+}$ and $PHLDA3^{-/-}$ mice. (*Left*) Sections were stained with antibody against insulin (β cell marker; red) and glucagon (α cell marker; green) and representative images are shown. Pancreas sections of three $PHLDA3^{+/+}$ and three $PHLDA3^{-/-}$ mice were analyzed. (*Right*) For each mouse, α-cell and β-cell areas were calculated from one pancreas section. (*$P < 0.05$.)

cell results in the elevation of blood glucose, and can thereby experimentally induce type I diabetes in mice. We analyzed blood glucose levels at the indicated times following STZ treatment, and STZ administration resulted in the effective elevation of blood glucose levels in wild-type mice, whereas elevation was diminished in $PHLDA3^{-/-}$ mice (Fig. 8*D*). When we calculated β cell and α cell areas in STZ-treated mice, we observed a significant increase in the area occupied by β cells in *PHLDA3*-deficient mice, showing that PHLDA3 is required for the efficient induction of β cell apoptosis by STZ (Fig. 8*E*). These results demonstrate that PHLDA3 controls Akt activity, cell size, and apoptosis of islet cells in vivo.

## Discussion

In this report, we have shown that PHLDA3 is a candidate tumor suppressor in PanNETs. We observed that the LOH of the *PHLDA3* gene locus in human PanNETs occurs at a remarkably high frequency and is comparable to that of the *MEN1* gene locus, the gene reported to be most frequently affected in PanNETs (15). We also showed that LOH at the *PHLDA3* gene locus is associated with disease progression and poor prognosis in PanNETs. In contrast, LOH/mutation of *MEN1* was found to be unrelated to the prognosis of PanNET patients, both in this and in a previous study (7). These results show that the PHLDA3-regulated tumor suppression pathway is relevant to the progression and malignant phenotype of PanNETs and the poor prognosis of PanNET patients. Because PHLDA3 is a repressor of Akt, we propose that inhibition of the Akt pathway would improve the prognosis of PanNET patients exhibiting LOH of *PHLDA3*. This possibility is supported by the reported clinical efficacy of the Akt pathway inhibitor Everolimus, which has been shown to improve the survival of PanNET patients significantly. Everolimus treatment was approved in Japan only from 2011, and therefore none of the patients in our study had received Everolimus. We speculate that patients who are positive for *PHLDA3* LOH and have a poor prognosis may benefit most from Everolimus treatment. Furthermore, determination of *PHLDA3* LOH status could serve as a diagnostic measure to select patients who should receive Everolimus. Thus, it will be important to conduct a prospective study to analyze the effect of Everolimus in patients with or without *PHLDA3* LOH.

We have shown that PHLDA3 regulates Akt activity and various Akt-regulated biological processes, i.e., cell proliferation, cell size, and apoptosis, in cultured cell lines and in vivo endocrine cells. Several laboratories have generated transgenic mice that specifically express active Akt in β cells (6, 16). These mice developed hyperplastic islets, but did not develop malignant PanNETs (17). Likewise, we have shown that loss of PHLDA3 and the resulting activation of Akt leads to hyperplastic islet development, but not to the development of PanNETs. Although Akt activation is observed in various cancers and contributes to tumorigenesis and tumor progression, the conclusion derived from these experiments is that activation of Akt pathway alone is insufficient to cause PanNETs unless combined with an oncogenic event in a second pathway. In human PanNETs, double LOH of *PHLDA3* and *MEN1* is frequently observed. In these cells, loss of PHLDA3 function, i.e., activation of Akt, is combined with loss of MEN1 function to promote PanNET tumorigenesis, and loss of PHLDA3 function particularly contributes to the progression of PanNETs. It would therefore be interesting to generate mice that are doubly deficient in *PHLDA3* and *MEN1* to analyze whether the islet phenotypes are more pronounced and the hyperplastic islets more prone to malignancy.

We observed hyperplastic islets in *PHLDA3* heterozygote (+/−) mice as well as *PHLDA3*-deficient (−/−) mice. This observation suggests that *PHLDA3* is haplo-insufficient for the suppression of endocrine cell proliferation. We have previously shown that PHLDA3 expression represses Akt activity in a dose-dependent manner, consistent with the possibility that loss of a single *PHLDA3* allele could lead to enhanced Akt activation and enhanced proliferation of endocrine cells (8). However, we have also shown that in human PanNETs, the *PHLDA3* locus undergoes methylation in addition to LOH, suggesting that two hits on the *PHLDA3* gene is required for human PanNET development. We assume that loss of both *PHLDA3* alleles, and consequent stronger activation of Akt, may be required to exert a tumorigenic phenotype. Future studies should examine the islet phenotypes of $PHLDA3^{+/-}$ and $PHLDA3^{-/-}$ in a $MEN1^{-/-}$ back-

ground. We expect that, in a *MEN1*$^{-/-}$ background, *PHLDA3*$^{-/-}$ mice would develop PanNETs more frequently than in *PHLDA3*$^{+/-}$ mice. In addition, because we found association of LOH at the *PHLDA3* locus in both nonfunctional and functional human PanNETs, whether nonfunctional PanNETs develop in these mice is an interesting issue.

We previously identified *PHLDA3* as a p53 target gene. In the present study, we show that the *PHLDA3* locus undergoes frequent LOH in PanNETs, a tumor type in which p53 mutations are rare (3, 7). Recently it has been reported that among the various target genes of p53, *PHLDA3* displays prominent tumor suppressor activity (18). Therefore, in tumors harboring a p53 mutation, loss of p53-regulated *PHLDA3* expression may significantly contribute to tumor progression, whereas in tumors without a p53 mutation, loss of the *PHLDA3* gene itself may drive oncogenesis. Interestingly, global methylation profiling of prostate cancer specimens has revealed significant methylation of the *PHLDA3* gene in these cancers (19). In addition, in the COSMIC database, 11 PHLDA3 mutations in several cancers are reported. All mutations are located within the PH domain of PHLDA3, and nonsynonymous mutations may result in loss of Akt repressing ability. Therefore, in addition to inactivation by methylation, these and other mutations that result in a functional loss of PHLDA3 may contribute to some cancers.

In summary, our results show that PHLDA3 is a novel tumor suppressor of PanNET, and PHLDA3 and MEN1 cooperatively suppress its development. PHLDA3 represses Akt activity in islet cells and hyperplastic islets are found in both *PHLDA3*$^{+/-}$ and *PHLDA3*$^{-/-}$ mice. Collectively, our data illustrates the importance of the PHLDA3-regulated tumor suppression pathway in PanNETs.

## Materials and Methods

**Cell Lines, Cell Culture, Transfection, Adenovirus Infection, and Soft Agar Colony Formation Assay.** Cell lines used in this study were: LNCaP (human prostate cancer), MDA-MB-M468 (human breast cancer), DLD1 (human colorectal cancer), H1299 (human lung NET), A99 (human PanNET, ref. 20), RIN (rat pancreatic β cell), and MIN6 (mouse pancreatic β cell). Cell culture and transfection was performed as described (21). The siRNAs were introduced using RNAiMAX (Invitrogen). ON-target plus control and ON-target plus PHLDA3-targeting siRNAs were purchased from Dharmacon Research. Adenovirus infection was performed using previously described adenoviruses expressing LacZ or N-terminally HA-tagged PHLDA3 (8). Everolimus (AdooQ BioScience) was added to cultures at the indicated concentrations. For soft agar colony formation assays, cells were seeded in 3-cm dishes with a bottom layer of 0.5% agarose and a top layer of 0.33% agarose, both in complete media. The assay was performed in triplicate for each sample. Colonies were photographed after 9 (H1299) or 10 (MIN6) days of incubation. Colonies were counted in three to five different views from each plate to calculate average values. The total numbers of colonies larger than 100 (MIN6) or 200 (H1299) pixels were counted per view.

**Western Blotting Analysis.** Cells were lysed in lysis buffer [50 mM Tris·HCl (pH 8.0), 1% Nonidet P-40, 250 mM NaCl, 50 mM NaF, 1 mM $Na_3VO_4$, 1 mM protease inhibitor (PMSF, aprotinin, leupeptin) and 1 mM DDT]. Whole cell lysates were subjected to protein quantification and analyzed by Western blotting. To detect PHLDA3, 20 μg of whole cell lysates (WCL) were loaded. To detect other proteins, 5 μg of WCL were loaded. Antibodies used in this study were: anti-Akt rabbit polyclonal antibody, anti-phospho-Akt (S473) rabbit monoclonal antibody, anti-p70S6K rabbit monoclonal antibody, anti-phospho-p70S6K (T389) rabbit polyclonal antibody, anti-phospho-S6 (S240/244) rabbit monoclonal antibody, anti-phospho-Gsk3β (S9) rabbit polyclonal antibody, anti-phospho-Mdm2 (S166) rabbit polyclonal antibody from Cell Signaling Technology, anti-actin mouse monoclonal antibody from SIGMA from Santa Cruz Biotechnology, anti-PHLDA3 goat polyclonal antibody from Abcam, anti-HA monoclonal antibody (clone 12CA) from Roche Diagnostics.

**Reverse Transcription and Real-Time PCR.** Reverse transcription was carried out using kits from Invitrogen following the manufacturer's instructions (SuperScript First-Strand Synthesis System for RT-PCR). Total RNA (0.2–5 μg) was used for reverse transcription. Reverse-transcribed cDNAs were subjected to real-time PCR, which was performed with a LightCycler 480 Instrument (Roche Diagnostics). For the detection of PHLDA3 (human; Hs00385313_m1, mouse; Mm00449846_m1, rat; rat; Rn01483684_m1), beta actin (mouse; Mm00607939_s1, rat; Rn00667869_m1) and GAPDH (human; Hs02758991_g1, mouse; Mm99999915_g1), TaqMan probe from Applied Biosystems was used.

**BrdU Incorporation Assay and Measurement of Cell Number.** BrdU-positive cells were quantified using the Ziva Ultrasensitive BrdU assay (Jaden BioScience). This assay detects the incorporation of BrdU using a labeled anti-BrdU antibody and detection substrate in an ELISA format. By this assay, a small fraction of proliferating cells within a large population of nonproliferating cells can be detected. Cell numbers were analyzed by using CellTiter-Glo Luminescent Cell Viability Assay (Promega). Using this assay, viable cells are determined by quantitation of ATP, an indicator of metabolically active cells.

**Flow Cytometry and TUNEL Assay.** Apoptosis of islet cells was quantitated by the TUNEL reaction using the In Situ Cell Death Detection kit, Fluorescein (Roche Diagnostics) followed by flow cytometry. Flow cytometry analysis was performed using a FACS Calibur instrument (Becton Dickinson).

**Tumor Samples Used in the Study, and DNA and RNA Extraction from Primary Tumor Samples.** The tumor samples used in this study were surgically resected at the National Cancer Center Hospital (44 samples; PanNET1-18, 24–47, 52, 53), Kyoto University Hospital (6 samples; PanNET19-23, 51), or Kagawa University Hospital (4 samples; PanNET 48–50, 54) between 1993 and 2012. Histological grading of the tumors were determined based on the classification of World Health Organization 2004. This study was approved by the Institutional Review Board of the National Cancer Center, Tokyo. Clinical and pathological data were obtained through a detailed retrospective review of the medical records of all patients with PanNET. Five-micrometer sections of paraffin-embedded tissues were subjected to DNA extraction. Total RNA was extracted from frozen normal pancreas and tumor samples using an RNeasy mini kit (Qiagen).

**Microsatellite Analysis.** Microsatellite analysis was performed basically as described (8). We used six primer pairs labeled with FAM that amplify microsatellite loci to achieve accurate detection of LOH at the *PHLDA3* locus (Fig. 1*A*). For the *MEN1* locus, three primer pairs were used (Fig. 2*A*). Amplified PCR products were analyzed with a 3100 automated sequencer (Applied Biosystems). Collected data were analyzed with GeneScan and Genotyper software (Applied Biosystems), and allele sizes and peak heights were calculated. The genotype was determined to be heterozygous if two bands of different sizes were obtained from normal tissues. A ratio of the two peaks in tumor DNA of less than 0.7 in comparison with the corresponding ratio of the two peaks in nontumor DNA was considered as allelic loss.

**5-aza-dC Treatment and Methylation-Specific PCR.** Cells were seeded at a density of $3 \times 10^5$ cells (H1299 and A99) or $3 \times 10^6$ (MIN6) cells per 10-cm dish on day 0 and treated with freshly prepared 5-aza-dC (Sigma-Aldrich) for 24 h on days 1, 3, and 5. After each treatment, cells were placed in fresh medium and harvested on day 6. Genomic DNA was extracted and subjected to bisulfite conversion using EZ DNA Methylation kit (Zymo research). Fully methylated controls were prepared by methylating genomic DNA with SssI methylase (New England Biolabs). Methylation-specific PCR (MSP) was performed basically as described (22). MSP was performed using the specific primer sets shown below. BS-F and R primers were used to amplify DNA with or without methylation. MSP-F and R primers were used to amplify methylated DNA.

BS-F: GTAGATAGAGTTTAGGGGAGTAAGAG

BS- R: CTCTACCCCAACTAACCCAACCC

MSP-F: GAGGGTTGGTTAGGGTAGGAATGTG

MSP-R: ACTCCCCTAAACTCTATCTACACAC

**Mice Used in This Study.** Generation of *PHLDA3*-deficient mice was reported (23). Briefly, a *PHLDA3*neo targeting vector was obtained by cloning a 6-kb upstream KpnI fragment and a 6-kb downstream HindIII/NotI fragment into pPNT1. The resulting deletion (nucleotides 579–2,096 of GenBank accession no. AF151099) eliminates all of exon 1 and part of exon 2, thus deleting the entire *PHLDA3* coding region. *PHLDA3*$^{-/-}$ mice were generated by crossing the heterozygotes. MEFs were isolated and maintained as described (24). Mouse experiments were performed in a specific pathogen-free environment at the National Cancer Center animal facility according to institutional guidelines, and all of the animal experiments were approved by the Committee for Ethics in Animal Experimentation at the National Cancer Center.

**Blood Glucose, Plasma Insulin Measurement, and Glucose Tolerance Tests.** Blood glucose levels were determined with blood samples from tail vein

punctures in mice using Glucose pilot (Aventir Biotech), according to the procedures specified by the manufacturer. Plasma insulin levels were determined with blood samples from tail vein punctures or inferior vena cava in mice by ELISA (Morinaga Institute of Biological Science), according to the procedures specified by the manufacturer. For glucose tolerance tests, mice were fasted overnight and blood was drawn from tail vein at 0, 15, 30, 45, 60, 90, and 120 min after i.p. injection of D-glucose (2 mg/g of body weight).

**Quantitative Measurement of Islet Morphology.** Islet area and islet nuclei number were measured from hematoxylin and eosin-stained pancreas sections and Ki67-positive cells were counted from immunohistochemically stained pancreas sections using TissueFAXS (TissueGnostics). Chromogranin A signal intensity was also measured using TissueFAXS. α and β cells areas were quantified by the number of pixels in each immunohistochemically stained area in images taken by fluorescence microscopy (Olympus IX2-DSU).

**Isolation of Rat and Mouse Primary Islets and Preparation of Primary Islet Cells.** The animal experiment was reviewed and approved by the Institutional Animal Care and Use Committee for Frontier Medical Sciences, Kyoto University. For isolation of rat islets, Lewis or Wistar rats (male, aged 9–11 wk, Shimizu Laboratory Supplies) were used. Islet isolation was performed according to previously described methods (25). Briefly, through midline laparotomy, 10 mL of a type XI collagenase solution (1200 CDU/mL, C9407, Sigma-Aldrich) was infused into the common bile duct that was ligated at the hepatic side before the inflow into the duodenum. The pancreases were removed and digested in a water bath set at 37 °C for 18 min. The digested pancreases were filtered with a stainless steel sieve to separate the islets, and purified using a discontinuous gradient solution (Dextran 70, 17–0280-02, Amersham). Mouse islets were isolated from 10- to 25-wk-old male animals by collagenase digestion of the pancreas, followed by purification using a Ficoll gradient. Islets were handpicked twice. The harvested islets were cultured in RPMI or CRML-1066 medium (11530, Gibco) supplemented with a 1% antibiotic–antimycotic solution (15240-062, Gibco) and 10% (vol/vol) FBS (12103-78P, JRH) in an incubator set at 5% (vol/vol) $CO_2$, 37 °C.

Primary islet cells were prepared by digesting the islets with Accutase for 15 min at 37 °C. Islet cells were washed with RPMI before use in experiments.

**Immunohistochemistry.** Immunohistochemistry (IHC) was performed basically according to the manufacturer's instructions. In brief, after deparaffinization, tissues sections underwent antigen retrieval by autoclaving slides for 5 min in 10 mM citrate buffer (pH 6.0). For fluorescent immunohistochemical staining of insulin, glucagon, and Glut2, nonspecific interactions were blocked for 30 min using a 5% (vol/vol) goat serum solution. The primary antibodies were: guinea pig anti-insulin polyclonal antibody (Abcam) diluted 1:400, mouse anti-glucagon monoclonal antibody (Sigma-Aldrich) diluted 1:750 and rabbit anti-Glut2 polyclonal antibody (Alpha Diagnostic) diluted 1:750 with Signal Enhancer HIKARI (Nacalai Tesque). These were applied to the slides and incubated overnight at 4 °C. As secondary antibodies, Alexa Fluor 488 goat anti-mouse IgG antibody (Invitrogen) diluted 1:500, Alexa Fluor 488 goat anti-rabbit IgG antibody (Invitrogen) diluted 1:500 and Alexa Fluor 546 goat anti-guinea pig IgG antibody (Invitrogen) diluted 1:1,000 with PBST-BSA were applied to the slides and incubated 3 h at room temperature. To detect Ki67- and Chromogranin A-positive cells, sections were pretreated with 0.3% $H_2O_2$ for inactivation of endogenous peroxidase. The primary antibody, rat anti-Ki67 monoclonal antibody (DakoCytomation) diluted 1:200, or rabbit anti-Chromogranin A polyclonal antibody (Thermo Scientific) diluted 1:200 with Signal Enhancer HIKARI were applied to the slides and incubated overnight at 4 °C. As secondary antibodies, Histofine Simple Stain MAX PO anti-rat IgG antibody (Nichirei Bioscience) or biotinylated anti-rabbit IgG antibody (VECTOR Laboratories) was used. We used 3,3′-diaminobenzidine tetrahydrochloride (DAB; Muto Pure Chemicals) as the substrate chromogen. The sections were counter stained with hematoxylin.

**STZ-Induced Diabetes.** Eleven- to 22-wk-old wild-type and *PHLDA3* knockout male mice were injected i.p. with 50 mg/kg streptozotocin daily for 5 consecutive days (Sigma-Aldrich) to produce β cell injury. On days 92, 93, 99, and 100, animals were killed.

**Statistical Analysis.** Data were calculated and shown as mean ± SD (for Figs. 4, 5 and *SI Appendix*, Fig. S3) or as mean ± SEM (Figs. 6–8 and *SI Appendix*, Figs. S7, S9, and S10*A*). Comparisons between the samples were performed by Student *t* test. Survival data were analyzed using XLStat software (version 2013.4.05; Addinsoft), and Kaplan–Meyer plots were drawn. Wilcoxon test was performed to assess the statistical significance of the difference between the survival curves. In Fisher's exact test, *P* values were obtained by using two tails. Statistical significance was defined as $P < 0.05$.

**ACKNOWLEDGMENTS.** We thank T. Niwa and T. Ushijima (National Cancer Center, Japan) for advice on methylation-specific PCR, Marc Lamphier for critical reading of the manuscript, Dr. Wanxing Cui for providing isolated human islets, and Drs. T. Yoshida and H. Sakamoto and National Cancer Center Research Core Facility (supported by National Cancer Center Research and Development Fund, 23-A-7) for the LOH analyses in this study. This study was supported by Grants-in-Aid for Scientific Research from the Ministry of Education, Culture, Sports, Science and Technology of Japan (23501279 and 26430133, to R.O.); New Energy and Industrial Technology Development Organization (NEDO) (09A02012a, to R.O.); research grants from Daiichi-Sankyo Foundation of Life Science (to R.O.); the Ichiro Kanehara Foundation (R.O.); Takeda Science Foundation (R.O.); Astellas Foundation for Research on Metabolic Disorders (R.O.); Foundation for Promotion of Cancer Research in Japan (R.O.); Extramural Collaborative Research Grant of Cancer Research Institute, Kanazawa University, Japan (to R.O.); Cooperative Research Program of Institute for Frontier Medical Sciences, Kyoto University, Japan (R.O.); and grants from the National Cancer Center Research and Development Fund (23-B-9, to R.O.; and 23-A-11, to T.T.).

1. Hauso O, et al. (2008) Neuroendocrine tumor epidemiology: Contrasting Norway and North America. *Cancer* 113(10):2655–2664.
2. Yao JC, et al. (2008) One hundred years after "carcinoid": Epidemiology of and prognostic factors for neuroendocrine tumors in 35,825 cases in the United States. *J Clin Oncol* 26(18):3063–3072.
3. de Wilde RF, Edil BH, Hruban RH, Maitra A (2012) Well-differentiated pancreatic neuroendocrine tumors: From genetics to therapy. *Nat Rev Gastroenterol Hepatol* 9(4):199–208.
4. Yao JC, et al.; RAD001 in Advanced Neuroendocrine Tumors, Third Trial (RADIANT-3) Study Group (2011) Everolimus for advanced pancreatic neuroendocrine tumors. *N Engl J Med* 364(6):514–523.
5. Elghazi L, Bernal-Mizrachi E (2009) Akt and PTEN: Beta-cell mass and pancreas plasticity. *Trends Endocrinol Metab* 20(5):243–251.
6. Tuttle RL, et al. (2001) Regulation of pancreatic beta-cell growth and survival by the serine/threonine protein kinase Akt1/PKBalpha. *Nat Med* 7(10):1133–1137.
7. Jiao Y, et al. (2011) DAXX/ATRX, MEN1, and mTOR pathway genes are frequently altered in pancreatic neuroendocrine tumors. *Science* 331(6021):1199–1203.
8. Kawase T, et al. (2009) PH domain-only protein PHLDA3 is a p53-regulated repressor of Akt. *Cell* 136(3):535–550.
9. Yang YM, et al. (2005) Chromosome 1q loss of heterozygosity frequently occurs in sporadic insulinomas and is associated with tumor malignancy. *Int J Cancer* 117(2):234–240.
10. Chen YJ, Vortmeyer A, Zhuang Z, Huang S, Jensen RT (2003) Loss of heterozygosity of chromosome 1q in gastrinomas: Occurrence and prognostic significance. *Cancer Res* 63(4):817–823.
11. Corbo V, et al. (2010) MEN1 in pancreatic endocrine tumors: Analysis of gene and protein status in 169 sporadic neoplasms reveals alterations in the vast majority of cases. *Endocr Relat Cancer* 17(3):771–783.
12. Yoo NJ, Kim YR, Lee SH (2011) Expressional and mutational analysis of PHLDA3 gene in common human cancers. *Pathology* 43(5):510–511.
13. Brenet F, et al. (2011) DNA methylation of the first exon is tightly linked to transcriptional silencing. *PLoS ONE* 6(1):e14524.
14. Lenzen S (2008) The mechanisms of alloxan- and streptozotocin-induced diabetes. *Diabetologia* 51(2):216–226.
15. Pannett AA, Thakker RV (1999) Multiple endocrine neoplasia type 1. *Endocr Relat Cancer* 6(4):449–473.
16. Bernal-Mizrachi E, Wen W, Stahlhut S, Welling CM, Permutt MA (2001) Islet beta cell expression of constitutively active Akt1/PKB alpha induces striking hypertrophy, hyperplasia, and hyperinsulinemia. *J Clin Invest* 108(11):1631–1638.
17. Vivanco I, Sawyers CL (2002) The phosphatidylinositol 3-Kinase AKT pathway in human cancer. *Nat Rev Cancer* 2(7):489–501.
18. Brady CA, et al. (2011) Distinct p53 transcriptional programs dictate acute DNA-damage responses and tumor suppression. *Cell* 145(4):571–583.
19. Mahapatra S, et al. (2012) Global methylation profiling for risk prediction of prostate cancer. *Clin Cancer Res* 18(10):2882–2895.
20. Yachida S, et al. (2011) Establishment and characterization of a new cell line, A99, from a primary small cell carcinoma of the pancreas. *Pancreas* 40(6):905–910.
21. Ozeki C, et al. (2011) Cancer susceptibility polymorphism of p53 at codon 72 affects phosphorylation and degradation of p53 protein. *J Biol Chem* 286(20):18251–18260.
22. Yamashita S, Tsujino Y, Moriguchi K, Tatematsu M, Ushijima T (2006) Chemical genomic screening for methylation-silenced genes in gastric cancer cell lines using 5-aza-2′-deoxycytidine treatment and oligonucleotide microarray. *Cancer Sci* 97(1):64–71.
23. Frank D, et al. (2002) Placental overgrowth in mice lacking the imprinted gene Ipl. *Proc Natl Acad Sci USA* 99(11):7490–7495.
24. Ohki R, et al. (2000) Reprimo, a new candidate mediator of the p53-mediated cell cycle arrest at the G2 phase. *J Biol Chem* 275(30):22627–22630.
25. Yang KC, et al. (2010) The cytoprotection of chitosan based hydrogels in xenogeneic islet transplantation: An in vivo study in streptozotocin-induced diabetic mouse. *Biochem Biophys Res Commun* 393(4):818–823.

Pathology International

*Pathology International* 2014; **64**: 39–44 doi:10.1111/pin.12131

Case Report

# Intraductal dissemination of papillary adenocarcinoma of the ampulla of Vater in the pancreatic duct

**Akiko Matsubara,[1,2] Satoshi Nara,[3] Shigeki Sekine,[1] Hidenori Ojima,[1] Tomoo Kosuge,[3] Kazuaki Shimada,[3] Ryoji Kushima,[2] Yae Kanai[1] and Nobuyoshi Hiraoka[1]**

[1]*Division of Molecular Pathology, National Cancer Center Research Institute,* [2]*Pathology and Clinical Laboratories, and* [3]*Hepato-Biliary and Pancreatic Surgery Division, National Cancer Center Hospital, Tokyo, Japan*

**It has been speculated that intraductal dissemination, via the pancreatic duct, bile duct, or mammary duct, is a unique form of cancer cell spread. However, clinical evidence to confirm this form of dissemination has been lacking. Here we report a case of papillary adenocarcinoma of the ampulla of Vater in which retrograde dissemination to the pancreatic duct was strongly suggested. A 79-year-old woman underwent pancreatoduodenectomy for a 22 mm microinvasive papillary adenocarcinoma of the ampulla. Multiple carcinomas *in situ* were found in the pancreatic duct distant from the ampulla. Seven months later, she underwent a second operation for a recurrent papillary adenocarcinoma at the pancreato-jejunal anastomosis showing exophytic and expansive growth into the jejunal lumen that connected to an intraductal adenocarcinoma in the pancreatic body. None of these tumors showed invasive growth, or vascular or neural invasion, being separate from each other but sharing identical histological, immunohistochemical, and molecular features; papillary growth, a pancreatobiliary phenotype, the same pattern of genomic loss of heterozygosity, and no mutation of the *KRAS*, *TP53*, and *GNAS* genes. These results imply that this papillary adenocarcinoma of the ampulla of Vater had disseminated to the pancreatic duct in a retrograde manner and recurred in the remnant pancreas.**

**Key words:** ampulla of Vater, intraductal dissemination, pancreatic duct, papillary adenocarcinoma

During tumor growth, cancer cells that have developed in the epithelial layer begin to invade by breaking through the basement membrane to extend into the surrounding stroma, followed by further continuous invasion. They can also spread discontinuously through metastasis or dissemination, which is usually achieved by carriage through the hematogeneous or lymphatic pathways, or within the peritoneal cavity. Similarly, dissemination of cancer cells via ducts such as the pancreatic duct or mammary duct would provide a further potential corridor for cancer cells in patients with pancreatic cancer and breast cancer. Empirically, several suspected cases of tumor spread or dissemination via the pancreatic or mammary duct have been reported, although pathologically proven cases have been very scant.[1]

Adenocarcinoma of the ampulla of Vater is a rare malignant epithelial tumor, with an incidence of 0.5–5% among all gastrointestinal malignancies.[2] Carcinoma of the ampulla of Vater usually spreads to neighboring tissue directly, as well as showing lymph node and distant metastasis. However, no proven case of dissemination via the pancreatic duct, bile duct, or digestive tract has been reported. Here we describe the first reported case of adenocarcinoma of the ampulla of Vater showing retrograde dissemination via multiple branches of the pancreatic duct.

## CLINICAL SUMMARY

A 79-year-old Japanese woman was admitted to our hospital with abdominal fullness, abdominal pain, and nausea. She had no significant medical history. Abdominal computed tomography (CT) revealed a 2.0 cm slightly enhanced mass in the ampulla of Vater, and dilation of the bile duct. Ultrasonography yielded similar findings. Serum examination revealed no elevation of any tumor marker levels. She underwent pylorus-preserving pancreatoduodenectomy for carcinoma of ampulla of Vater and reconstruction of duodenal-jejunal and pancreato-jejunal anastomoses. The surgery was uneventful, and the postoperative course was good. Seven month later, abdominal CT revealed a 5.0 cm

Correspondence: Nobuyoshi Hiraoka, MD, PhD, Division of Molecular Pathology, National Cancer Center Research Institute, 5-1-1 Tsukiji, Chuo-ku, Tokyo 104-0045, Japan. Email: nhiraoka@ncc.go.jp

Received 25 October 2013. Accepted for publication 16 December 2013.

tumor at the site of the pancreato-jejunal anastomosis. A second operation was performed to resect the pancreatic body and tail with partial anastomosis of the jejunum to the pancreatic body. The operation was uneventful, and no recurrence has been observed during 22 months of follow-up.

## PATHOLOGICAL FINDINGS

### First surgical specimen

Surgically resected specimens were observed macroscopically, fixed in 10% formalin, and cut into serial slices 5 mm thick, almost frontally in the specimen. All of these sections were then subjected to detailed histopathological examination. On gross examination, the ampulla of Vater was swollen by a protruding tumor (Fig. 1a) and the tumor had grown expansively at the ampulla (Fig. 1b). Histologically, the tumor had proliferated and filled the lumen of the common channel with slight extension to the ampullary pancreatic and bile ducts without invasion to the surrounding organs (Fig. 1c), although microinvasion to the Oddi sphincter was evident (Fig. 1d). The tumor consisted of atypical tall columnar epithelial cells with marked cytological atypia, and showing a markedly complex papillary architecture (Fig. 1e), indicating a diagnosis of microinvasive papillary adenocarcinoma arising in association with pancreatobiliary (PB)-type non-invasive papillary neoplasm. The tumor measured 22 × 15 × 15 mm and had no evidence of lymphatic, venous, or neural invasion, or nodal metastasis.

Multiple carcinomas *in situ* (CISs) were seen in the pancreatic ducts (Fig. 1f,g) without any atypical epithelial hyperplasia (corresponding to a low grade pancreatic intraepithelial neoplasm) around them. Each CIS was microscopic in dimension, the largest one measuring 3 mm. Multiple CISs were scattered in the pancreatic head and tended to be localized at the periphery of pancreatic lobules. The distance between the CISs and the ampullary tumor was at least 1.2 cm. One of the CISs showed microinvasion into the surrounding stroma (Fig. 1g). It was highly suspected that CISs remained in the remnant pancreas, since they were seen in the surgical margin.

### Second surgical specimen

The 47 × 45 × 25 mm exophytic tumor projecting into the jejunal lumen at the pancreato-jejunal anastomosis was lobulated, crumbly, and polypoid, and covered with necrotic debris (Fig. 1h). The cut surface was dark brownish and hemorrhagic, and in addition, it was possible to squeeze white medullary tumors from the cut surface of the pancreatic ducts (Fig. 1i). Histologically, both the exophytic polypoid tumor and the intraductal proliferating tumors in the pancreatic ducts in the pancreatic body were PB-type papillary adenocarcinoma, similar to the ampullary tumor (Fig. 1j,k). The polypoid tumor grew expansively into the surrounding stroma, being connected to the intraductal tumors in the pancreatic ducts (Fig. 1l,m). The tumor showed no evidence of lymphatic, venous, or neural invasion, or nodal metastasis.

### Immunohistochemical analysis

Immunohistochemistry was carried out on formalin-fixed, paraffin-embedded tissue sections as described previously,[3] using antibodies shown in Table 1. The ampullary tumor and the CISs in the pancreatic ducts were positive for MUC1, MUC5AC, and MUC6, and negative for MUC2 and CD10. The recurrent tumor at the pancreato-jejunal anastomosis and the intraductal tumor in the pancreatic body showed identical profiles. All of the above tumors showed a tumor cell phenotype compatible with the PB type.

### Molecular analysis

We analyzed gene mutations and loss of heterozygosity (LOH) in the ampullary tumor, six independent CIS lesions selected randomly, and the recurrent tumor at the pancreato-jejunal anastomosis. Mutation analyses were performed as described previously,[4] and the PCR primers used in this study were shown in Table 2. LOH was analyzed as described previously.[5] Genomic DNA was amplified by PCR using oligonucleotide primers for 14 microsatellite markers: BAT25 (4q12), BAT40 (1p13.1), D16S408 (16q), D16S168 (16q21 to 22.1), IFNA (9q22), D18S69 (18q21), UT762 (21), ACTBP2 (6q), AR (X), DRPLA (12p13.31), D16S409 (16q), D16S410 (16p), D17S261 (17p12 to 11.1), and BAT26 (2p22 to 21). All of the tumors showed 4 retention of heterozygosity (IFNA, ACTBP2, DRPLA, and D16S409) and 3 LOH (D18S69, AR, and D17S261) among seven informative polymorphic genome loci within a total of 14 loci tested (Fig. 2); none of the tumors showed mutations of the *KRAS*, *TP53*, and *GNAS* genes These results strongly suggested that the ampullary tumor, multiple lesions of CIS in the pancreatic ducts and ductules, and the recurrent tumors in the pancreatic body were identical.

## DISCUSSION

Intraductal dissemination as a unique mode of cancer cell spread has been speculated for at least four decades. Transductal dissemination of cancer cells injected into the pancreatic duct has been observed in a rabbit model.[6]

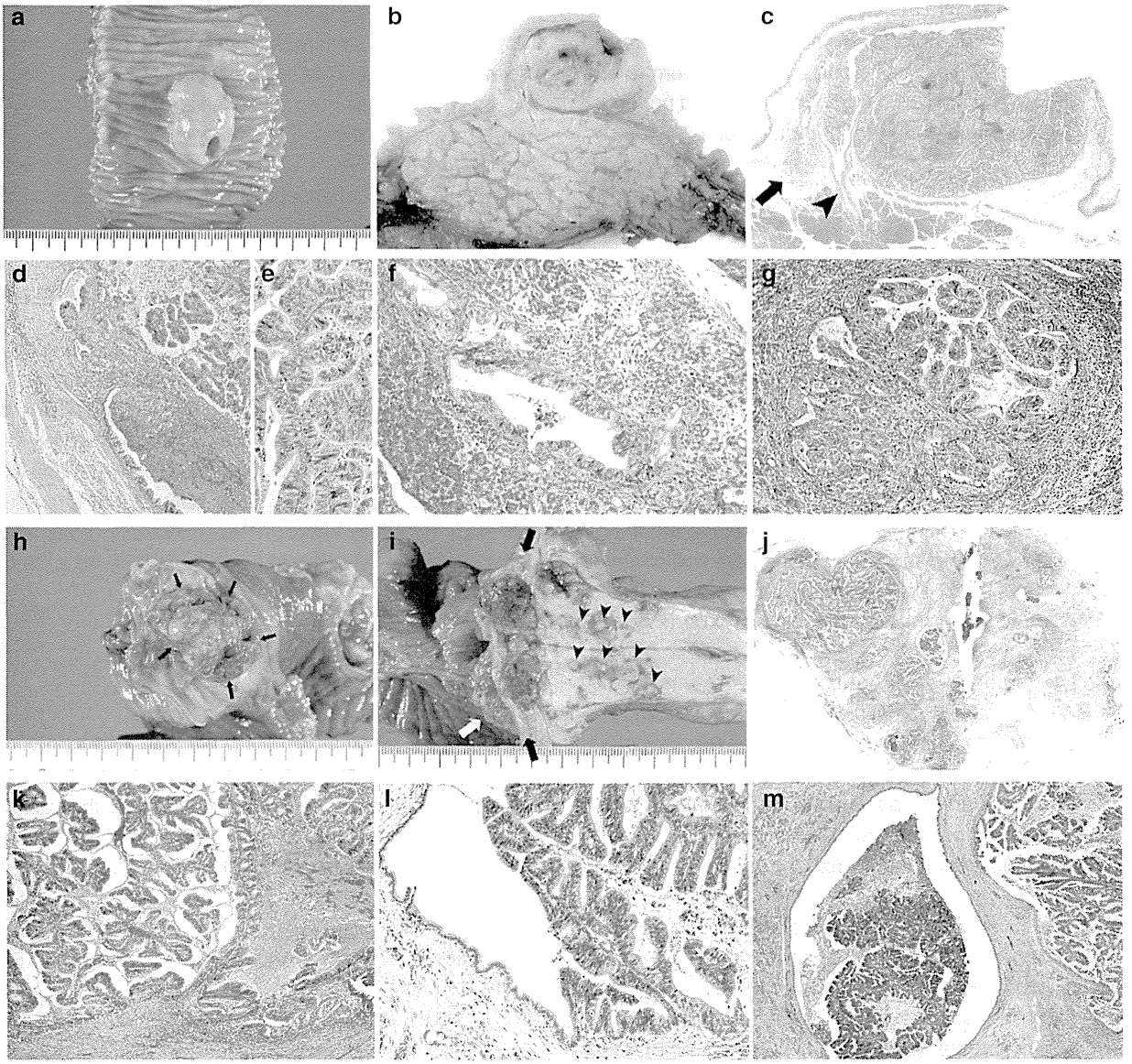


**Figure 1** Gross and microscopic appearance of the specimen obtained by pancreatoduodenectomy (**a–g**). (**a**) On the luminal surface of the fresh duodenum, the ampulla of Vater is swollen by a 3 cm protruding tumor covered by intact duodenal mucosa, without tumor exposure. (**b**) In the frontally cut surface of the fixed specimen, the white, solid, and well demarcated tumor is seen to be localized in the ampulla of Vater. No tumor is evident in the pancreas. (**c**) Loupe view of the ampulla of Vater. The tumor has grown expansively in the common channel with a papillary structure that spreads slightly to both the ampullary bile duct (arrow) and the ampullary pancreatic duct (arrow head). The tumor is well demarcated and covered by the Oddi sphincter. (**d** and **e**) Medium-power (**d**) and high-power (**e**) view of the ampullary tumor. The tumor consists of atypical tall columnar epithelial cells with marked cytological atypia showing a markedly complex papillary architecture (**e**), being invasive to the Oddi sphincter at a few points, but not beyond it (**d**). (**f** and **g**) There are multiple lesions of carcinoma *in situ* (CIS) in the pancreatic ducts and ductules in the pancreatic head. The markedly atypical tall columnar cells have proliferated with low papillary features, and microinvasion is evident in one of the lesions (**g**). (**h–m**) Gross and microscopic features of the specimen obtained by surgical resection of the remnant pancreatic body and tail with the anastomosed jejunum. (**h**) In the luminal surface of the fresh jejunum, there is a protruding tumor at the pancreato-jejunal anastomosis, which shows exophytic, lobulated, crumbly, and polypoid features and is covered by hemorrhagic and necrotic debris on the surface. (**i**) In the horizontally cut surface of the fresh jejunum (black arrow) and pancreatic body and tail, the exophytically growing tumor (white arrows) is dark brownish, hemorrhagic, fragile, and well demarcated. Many white, hemorrhagic, and medullary tumors (arrow heads) have squeezed out from the cut surface of the pancreatic ducts in a 'tooth paste'-like manner in the pancreatic body. (**j**) Loupe view of the pancreatic body (sagittal section). The papillary tumor has proliferated and fills the cystically dilated pancreatic ducts, the surrounding pancreatic parenchyma having been replaced by fibrous tissue with chronic inflammation. (**k–m**) Low-power (**k**) and medium-power (**l, m**) views of the intraductal proliferating tumor in the pancreatic body. The exophytic polypoid tumor and the proliferating tumors in the pancreatic ducts are connected, and both tumors show a markedly complex papillary architecture and cytological atypia (**l**), quite similar to the histology of the ampullary tumor. Tumor cells have replaced the ductal covering epithelia (**l**), and the tumor cells are floating and proliferating in a papillary manner in the pancreatic ducts (**m**).

**Table 1** Primary antibodies used in the immunohistochemistry

| Antigens | Clone names | Working dilution | Antigen retrieval | Source |
|---|---|---|---|---|
| MUC1 | Ma695 | 1:100 | A/C (Cit)† | Leica Biosystems, Newcatsle, UK |
| MUC5AC | CLH2 | 1:200 | A/C (Cit)† | Leica Biosystems |
| MUC6 | CLH5 | 1:100 | A/C (Cit)† | Leica Biosystems |
| MUC2 | Ccp58 | 1:200 | A/C (Cit)† | Leica Biosystems |
| CD10 | 56C6 | 1:200 | A/C (Cit)† | Leica Biosystems |

†A/C (Cit): autoclave in citrate buffer (pH 6.0).

**Table 2** Sequencing primers

| Gene | Region | Forward 5′-3′ | Reverse 5′-3′ |
|---|---|---|---|
| KRAS | exon 2 | AGGCCTGCTGAAAATGACTG | GGTCCTGCACCAGTAATATGCA |
| | exon 6 | AGAGACGACAGGGCTGGTT | CTTAACCCCTCCTCCCAGAG |
| TP53 | exon 7 | CCTGCTTGCCACAGGTCT | GTGTGCAGGGTGGCAAGT |
| | exon 8 | TTCCTTACTGCCTCTTGCTTC | GCTTCTTGTCCTGCTTGCTT |
| GNAS | exon 8 | ACTGTTTCGGTTGGCTTTGGTGA | AGGGACTGGGGTGAATGTCAAGA |
| | exon 9 | GACATTCACCCCAGTCCCTCTGG | GAACAGCCAAGCCCACAGCA |

Empirically, several cases suspected to have involved tumor dissemination via the ducts of the mammary gland[7] and pancreas[6] have been reported. However, there was no firm clinical evidence to support this possibility except for only a case of acinar cell carcinoma that showed multiple intraductal dissemination from the tail to the head of the pancreas.[1] Clearly, it is necessary to confirm unequivocally that this mode of cancer cell spread occurs. However, appropriate cases that would allow this to be confirmed are very rare. Such cases would need to involve a non-invasive primary cancer of the pancreatic duct unassociated with any lymphatic or venous invasion, and multiple intraductal cancer foci, all of which are identical.

In the present case, the ampullary tumor and multiple small foci of CIS in the pancreatic ducts were non-invasive or microinvasive and lacked any lymphatic, venous, or neural invasion. The recurrent tumors in the pancreatic body also showed expansive growth and no lymphatic, venous, or neural invasion. These tumors may have been multicentrically developing primary tumors or a primary tumor with associated metastatic tumors. We considered the latter scenario to be more likely because all the tumors were discrete but shared identical histological, immunohistochemical, and molecular features, i.e., all showed intraductal papillary growth, a pancreatobiliary tumor cell phenotype, and the same pattern of LOH without mutations of the *KRAS*, *TP53*, and *GNAS* genes. The apparently larger size of the tumor in the ampulla of Vater allowed us to speculate that this was the primary. The *KRAS* and *TP53* gene mutations are the most important drivers for the development of ductal adenocarcinoma of the pancreas,[8] being detectable in more than 95% and 75% of cases, respectively,[8] compared with 28–46%[9,10] and 53–94%[11,12] of ampullary carcinomas, respectively. These findings further support our speculation that the primary tumor developed in the ampulla of Vater. If so, the multiple CISs and the recurrent tumors were thought to be metastatic lesions, although none of the recurrent tumors in the pancreatic body had any lymphatic, venous, or neural invasion. It was thought that retrograde intraductal dissemination was the most probable explanation for the mode of cancer spread.

Ohike *et al.* have proposed the intra-ampullary papillary-tubular neoplasm (IAPN) of the ampulla, representing the intra-ampullary counterpart of intraductal papillary mucinous neoplasm (IPMN) of the pancreas.[13] Recently, the *GNAS* mutation has been shown to be characteristic of IPMN.[14,15] Our present case fits the category of IAPN, although no *GNAS* mutation was detected. However, absence of *GNAS* mutations in IAPN is still inadmissible, as many more cases need to be analyzed to determine the true frequency of *GNAS* mutation.

In conclusion, we have presented a case of microinvasive papillary adenocarcinoma at the ampulla of Vater in which it was strongly suggested that the tumor cells had disseminated retrogradely to the pancreatic ducts and ductules from the primary, and recurred in the remnant pancreas after pancreatoduodenectomy. The case appears to be unique and valuable for considering whether cancer cells can disseminate via the pancreatic duct and its branches.

## ACKNOWLEDGMENTS

The authors wish to thank Ms. Rie Yamazaki-Itoh and Reiko Ogawa for excellent technical assistance. This work was supported by a Grant-in-Aid for Third Term Comprehensive 10-year Strategy for Cancer Control from the Ministry of Health, Labor and Welfare of Japan (NH) and the National Cancer Center Research and Development Fund (NH).

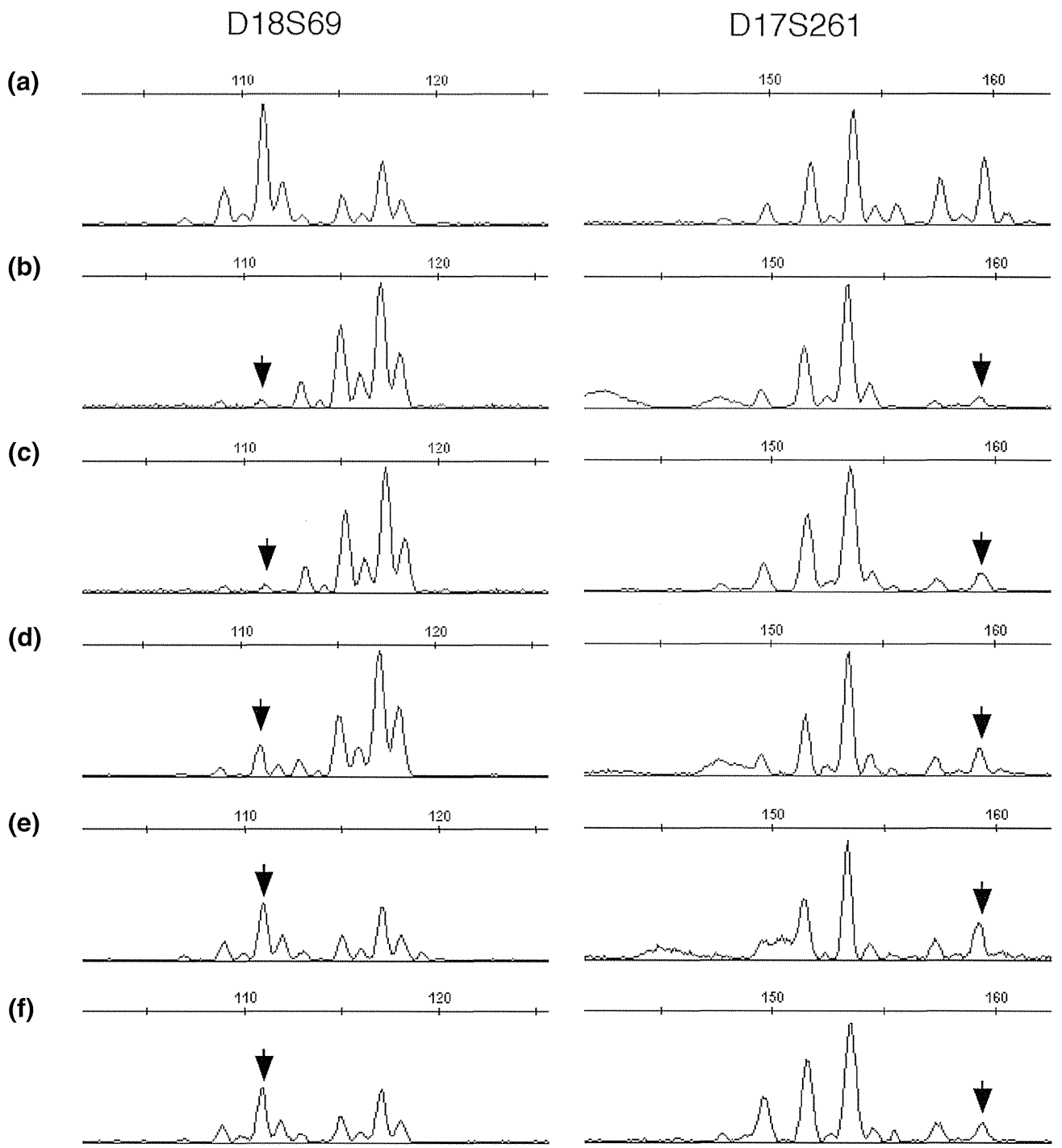


**Figure 2** Example results from loss of heterozygosity (LOH) analyses. DNA samples obtained from (**a**) the normal pancreas, (**b**) microinvasive papillary adenocarcinoma of the ampulla of Vater, (**c**) the recurrent papillary adenocarcinoma at the pancreato-jejunal anastomosis, and (**d–f**) three independent small foci of carcinoma *in situ* (CIS) in the pancreatic head were amplified with the markers D18S69 (left column) and D17S261 (right column). Allele sizes (bp) are indicated on the top horizontal axis. LOH was identified when the relative intensity of one allele was reduced by more than 70% in an informative case (arrows).

## REFERENCES


1 Ban D, Shimada K, Sekine S *et al.* Pancreatic ducts as an important route of tumor extension for acinar cell carcinoma of the pancreas. *Am J Surg Pathol* 2010; **34**: 1025–36.
2 Albores-Saavedra J, Hruban RH, Klimstra DS, Zamboni G. Invasive adenocarcinoma of the ampullary region. In: Bosman FT, Carneiro F, Hruban RH, Theise ND, eds. *WHO Classification of Tumours of the Digestive System*. Lyon: International Agency of Research on Cancer, 2010; 87–91.
3 Hiraoka N, Yamazaki-Itoh R, Ino Y *et al.* CXCL17 and ICAM2 are associated with a potential anti-tumor immune response in early intraepithelial stages of human pancreatic carcinogenesis. *Gastroenterology* 2011; **140**: 310–21.
4 Matsubara A, Sekine S, Kushima R *et al.* Frequent GNAS and KRAS mutations in pyloric gland adenoma of the stomach and duodenum. *J Pathol* 2013; **229**: 579–87.
5 Kondo Y, Kanai Y, Sakamoto M, Mizokami M, Ueda R, Hirohashi S. Genetic instability and aberrant DNA methylation in chronic hepatitis and cirrhosis—A comprehensive study of loss of heterozygosity and microsatellite instability at 39 loci and DNA hypermethylation on 8 CpG islands in microdissected specimens from patients with hepatocellular carcinoma. *Hepatology* 2000; **32**: 970–9.
6 Fujita N, Nakase A. Experimental study of transductal dissemination of cancer of the pancreas. *Gastroenterol Jpn* 1977; **12**: 224–9.
7 Morimoto T, Komaki K, Inui K *et al.* Involvement of nipple and areola in early breast cancer. *Cancer* 1985; **55**: 2459–63.
8 Iacobuzio-Donahue CA, Velculescu VE, Wolfgang CL, Hruban RH. Genetic basis of pancreas cancer development and progression: Insights from whole-exome and whole-genome sequencing. *Clin Cancer Res* 2012; **18**: 4257–65.
9 Schonleben F, Qiu W, Allendorf JD, Chabot JA, Remotti HE, Su GH. Molecular analysis of PIK3CA, BRAF, and RAS oncogenes in periampullary and ampullary adenomas and carcinomas. *J Gastrointest Surg* 2009; **13**: 1510–6.
10 Wagner PL, Chen YT, Yantiss RK. Immunohistochemical and molecular features of sporadic and FAP-associated duodenal adenomas of the ampullary and nonampullary mucosa. *Am J Surg Pathol* 2008; **32**: 1388–95.
11 Imai Y, Oda H, Tsurutani N, Nakatsuru Y, Inoue T, Ishikawa T. Frequent somatic mutations of the APC and p53 genes in sporadic ampullary carcinomas. *Jpn J Cancer Res* 1997; **88**: 846–54.
12 Scarpa A, Capelli P, Zamboni G *et al.* Neoplasia of the ampulla of Vater. Ki-ras and p53 mutations. *Am J Pathol* 1993; **142**: 1163–72.
13 Ohike N, Kim GE, Tajiri T *et al.* Intra-ampullary papillary-tubular neoplasm (IAPN): Characterization of tumoral intraepithelial neoplasia occurring within the ampulla: A clinicopathologic analysis of 82 cases. *Am J Surg Pathol* 2010; **34**: 1731–48.
14 Furukawa T, Kuboki Y, Tanji E *et al.* Whole-exome sequencing uncovers frequent GNAS mutations in intraductal papillary mucinous neoplasms of the pancreas. *Sci Rep* 2011; **1**: 161.
15 Wu J, Matthaei H, Maitra A *et al.* Recurrent GNAS mutations define an unexpected pathway for pancreatic cyst development. *Sci Transl Med* 2011; **3**: 92ra66.

OPEN ACCESS Freely available online

PLOS | ONE

# Metabolomics Evaluation of Serum Markers for Cachexia and Their Intra-Day Variation in Patients with Advanced Pancreatic Cancer

**Yutaka Fujiwara[1*¤], Takashi Kobayashi[2], Naoko Chayahara[1], Yoshinori Imamura[1], Masanori Toyoda[1], Naomi Kiyota[1], Toru Mukohara[1,3], Shin Nishiumi[2], Takeshi Azuma[2], Masaru Yoshida[2,4], Hironobu Minami[1,3]**

**1** Division of Medical Oncology/Hematology, Kobe University Graduate School of Medicine, Kobe, Japan, **2** Division of Gastroenterology, Kobe University Graduate School of Medicine, Kobe, Japan, **3** Cancer Center, Kobe University Hospital, Kobe, Japan, **4** Division of Metabolomics Research, Kobe University Graduate School of Medicine, Kobe, Japan

## Abstract

***Purpose:*** Cancer cachexia is a multifactorial syndrome characterized by progressive loss of weight and muscle atrophy. Using metabolomics, we investigated serum markers and their intra-day variation in advanced pancreatic cancer patients with cachexia.

***Methods:*** Patients were enrolled in two groups: those with or without cachexia. Blood samples collected at 6:30 AM, 11:30 AM, 4:30 PM, and 9:30 PM were analyzed using metabolomics, and serum levels of IL-6, TNF-α, and leptin were measured and compared between the two groups. Intra-day variation was then evaluated.

***Results:*** Twenty-one patients were enrolled in total. In the cachexia group (n = 9), median body weight loss rate over 6 months was greater, performance status was poorer, and anorexia was more severe than in the non-cachexia group (n = 12). Each metabolites level showed substantial intra-day variation, and some of them displayed significant differences between the two groups. Levels of paraxanthine remained markedly lower in the cohort with cachexia at all measurement points. Besides, median IL-6 and TNF-α levels appeared higher and leptin concentration appeared lower in the cachexia group, albeit without statistical significance.

***Conclusion:*** Some metabolites and some serological marker levels were affected by cancer cachexia. Although paraxanthine levels were consistently lower in patients with cachexia, we identified that many metabolites indicated large intra- and inter-day variation and that it might be necessary to pay attention to intra-day variation in metabolomics research.

**Citation:** Fujiwara Y, Kobayashi T, Chayahara N, Imamura Y, Toyoda M, et al. (2014) Metabolomics Evaluation of Serum Markers for Cachexia and Their Intra-Day Variation in Patients with Advanced Pancreatic Cancer. PLoS ONE 9(11): e113259. doi:10.1371/journal.pone.0113259

**Editor:** Antonio Gonzalez-Bulnes, INIA, Spain

**Received** July 13, 2014; **Accepted** October 21, 2014; **Published** November 20, 2014



**Funding:** This study was supported by a grant for Research on Applying Health Technology from the Ministry of Health, Labour, and Welfare of Japan. However, the funders had no role in study design, data collection and analysis, decision to publish, or preparation of the manuscript.

**Competing Interests:** The authors have declared that no competing interests exist.

* Email: yutakafu@ncc.go.jp

¤ Current address: Division of Investigational Cancer Therapeutics, Exploratory Oncology Research & Clinical Trial Center, National Cancer Center Hospital, Tokyo, Japan

## Introduction

Cachexia is a multifactorial syndrome characterized by progressive loss of weight and muscle atrophy that cannot be fully reversed by conventional nutritional support, thereby leading to progressive functional impairment [1]. Its pathophysiology is considered to involve a negative protein and energy balance driven by a variable combination of reduced food intake and abnormal metabolism. The agreed diagnostic criterion for cachexia is weight loss of greater than 5%, or weight loss greater than 2% in individuals already showing depletion, according to current body weight and height (body mass index $<20$ kg/m$^2$) or skeletal muscle mass [2].

Cachexia is reported in approximately 80% of advanced pancreatic cancer patients who typically develop a decreased dietary intake and a range of symptoms such as anorexia, early satiety, anxiety, and depression [3]. Cachexia has been shown to worsen prognosis and has also been associated with impairment of physical function, increased psychological distress, a reduction in tolerance of and response to therapy, a decrease in quality of life, and reduced duration of survival [4,5]. However, while substantial research is currently focused on determining the mechanism behind cachexia development, no precise understanding has yet been obtained.

Fasting hormones, such as leptin and ghrelin; pro-inflammatory cytokines, such as tumor necrosis factor-alpha (TNF-α), interferon gamma, and interleukin 6 (IL-6); insulin-like growth factor-1 (IGF-1); and the tumor-secreted proteolysis-inducing factor have all been implicated to some extent in cachexia development [6–9]. An

improved understanding of the integrative physiology of cancer cachexia may thus yield further novel therapeutic approaches.

Metabolomics (metabolome analysis) may prove useful in identifying the dynamic metabolic response of a living system to pathophysiological stimuli [10,11]. In metabolite profiling, the selected metabolites in a particular environment are identified and then subjected to quantitative or semi-quantitative assessment. This approach is useful for facilitating understanding of known metabolic pathways and biological alterations in mammalian homeostasis and living systems in pathophysiology [12].

Metabolism is known to be subject to circadian rhythms. The circadian timekeeping system in mammalian homeostasis is a hierarchical multi-oscillator network, with the suprachiasmatic nucleus acting as the central pacemaker [13,14], synchronizing to daily light-dark cycles and coordinating circadian metabolism and physiology. A comprehensive understanding of the pathophysiology of cancer cachexia may require consideration of the influence of intra-day variation [15].

Here, we investigated the difference in serum metabolite levels in pancreatic cancer patients with and without cachexia and analyzed the pattern and intra-day variation in metabolite levels using metabolomics.

## Methods

### Patient selection criteria

The study (trial registration ID: UMIN000002384) was conducted in hospitalized patients at Kobe University Hospital with pancreatic cancer that was locally advanced or metastatic and not amenable to curative surgical resection. Additional eligibility criteria were age ≥20 years, histologically confirmed adenocarcinoma or adenosquamous carcinoma of the pancreas, and adequate organ function (serum total bilirubin <1.5× upper limit of normal [ULN], aspartate aminotransferase [AST] <2.5×ULN, alanine aminotransferase [ALT] <2.5×ULN, and serum creatinine <1.5×ULN). No chemotherapy in the previous 7 days, no surgery or definitive irradiation in the previous 4 weeks, and palliative irradiation in the previous 2 weeks were permitted. Other exclusion criteria included active multiple primary cancer, serious pre-existing medical condition such as uncontrolled infection, diabetes mellitus, and concomitant use of steroids.

To discern small variations in metabolites, this study included cohorts with and without cachexia, defined as follows: the cohort with cachexia included those with an Eastern Cooperative Oncology Group performance status (ECOG PS) 1 to 4, grade 1 to 4 anorexia, and weight loss greater than 10% over the past 6 months; while that without cachexia included patients with a ECOG PS 0 to 2, grade 0 to 1 anorexia, serum albumin levels exceeding 3.5 mg/dL, and weight loss less than 5% over the past 6 months. Patients who didn't meet these cohort criteria were also excluded in this study.

All patients provided written informed consent, and study approval was obtained from the Institutional Review Board of Kobe University Hospital.

### Objectives and outcomes

The objective of this observational study was to investigate the difference in serum metabolite levels between pancreatic cancer patients with and without cachexia and to explore the pattern and intra-day variations in metabolite levels using metabolomics. Eligible subjects were assigned to either cohort with cachexia or that without cachexia. Primary endpoint was identification of cachexia-related metabolites using metabolomics. Secondary endpoints were intra-day variation in the metabolites involved in cachexia and changes in the level of serological markers involved in cachexia, such as inflammatory cytokines (e.g. IL-6, TNFα) and leptin, in the presence or absence of cachexia. Patient characteristics and medication information were recorded throughout the study. Adverse events were evaluated using the CTCAE v4.0.

The present study featured 10 subjects per group, as although this study was exploratory in nature and therefore involved no statistical rationale for sample size calculation, preceding studies on metabolomics have indicated significant results with a sample size of approximately 10 subjects per group. However, if a more useful analysis method found is found that may be implemented in the study, the analysis methods may be altered and the necessary sample size recalculated.

### Serum collection and preparation

Blood samples from hospitalized subjects were collected at 6:30 AM (after waking in early morning), 11:30 AM (late morning), 4:30 PM (early evening), and 9:30 PM (before retiring at night) at equal intervals in a single day to analyze intra-day variation. After collection of whole blood, samples were allowed to clot at room temperature, and serum was separated by centrifugation at 3,000×g for 10 min at 4°C and stored at −80°C until use.

To extract low-molecular-weight metabolites, 50 μl of serum was mixed with 250 μl of a solvent mixture (MeOH: $H_2O$:$CHCl_3$ = 2.5:1:1) containing 10 μl of 0.5 mg/ml 2-isopropylmalic acid (Sigma-Aldrich, Tokyo, Japan) dissolved in distilled water, and then the solution was shaken at 1,200 rpm for 30 min at 37°C before being centrifuged at 16,000×g for 5 min at 4°C. A total of 225 μl of the obtained supernatant was transferred to a clean tube, and 200 μl of distilled water was added. After mixing, the solution was centrifuged at 16,000×g for 5 min at 4°C, and 250 μl of the resultant supernatant was transferred to a clean tube before being lyophilized using a freeze dryer. For oximation, 40 μl of 20 mg/ml methoxyamine hydrochloride (Sigma-Aldrich) dissolved in pyridine was mixed with a lyophilized sample, and the mixture was shaken at 1,200 rpm for 90 min at 30°C. N-methyl-N-trimethylsilyltrifluoroacetamide (MSTFA; 20 μl) (GL Science, Tokyo, Japan) was then added for derivatization, and the mixture was incubated at 1,200 rpm for 30 min at 37°C. The mixture was then centrifuged at 16,000×g for 5 min at 20°C, and the resultant supernatant was subjected to gas chromatography-mass spectrometry (GC/MS) measurement.

Serum leptin levels were measured via radioimmunoassay as described previously in SRL Inc. (Tokyo, Japan) [16,17]. The limit of sensitivity was 0.5 ng/ml, and the intra- and interassay coefficients of variation both ranged from 2.5% to 5.0% over the sample concentration range. Serum IL-6 was detected using a Chemiluminescent Enzyme Immunoassay from SRL Inc. (Tokyo, Japan) [18]. The limit of sensitivity was 4.0 pg/ml, and the intra- and interassay coefficients of variation ranged from 2.2% to 3.8% and 3.6% to 8.6%, respectively, over the sample concentration range. Serum TNFα was detected using an Enzyme-Linked ImmunoSorbent Assay from SRL Inc. (Tokyo, Japan). Assay results ranged from 0.6 to 2.8 pg/ml.

### GC/MS analysis and data processing

GC/MS analysis was performed using a GCMS-QP2010 Ultra (Shimadzu Co., Kyoto, Japan) with a fused silica capillary column (CP-SIL 8 CB low bleed/MS; inner diameter, 30 mm×0.25 mm; film thickness, 0.25 μm; Agilent Co., Palo Alto, CA, USA), in accordance with a previously described method [19]. The front inlet temperature was 230°C, and the flow rate of helium gas through the column was 39.0 cm/sec. The column temperature was held at 80°C for 2 min and then raised by 15°C/min to

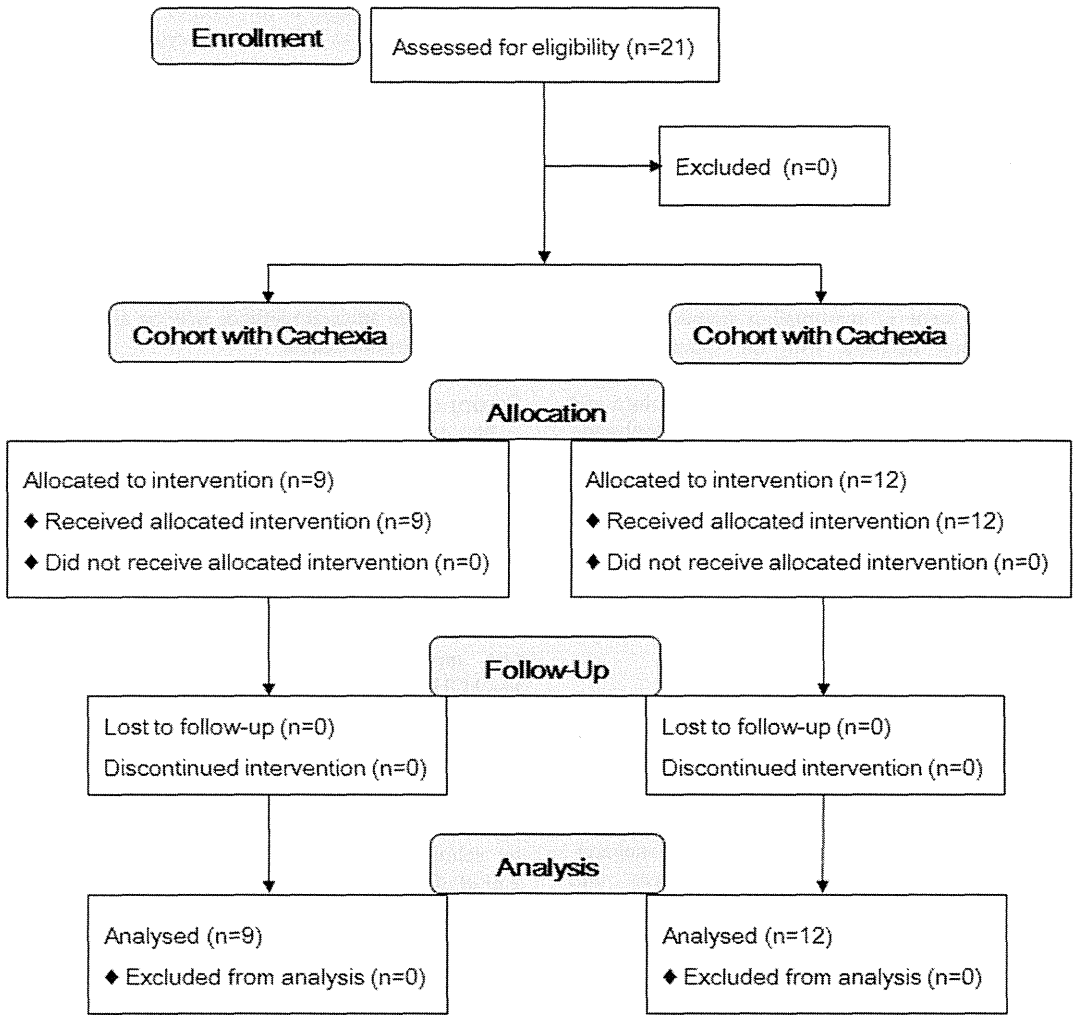


**Figure 1. CONSORT Flow Diagram.**
doi:10.1371/journal.pone.0113259.g001

330°C and held there for 6 min. The transfer line and ion-source temperatures were 250°C and 200°C, respectively. Twenty scans per second were recorded over the mass range 85–500 m/z using the Advanced Scanning Speed Protocol (ASSP, Shimadzu Co.).

Data processing was performed in accordance with the methods described in previous reports [19,20]. Briefly, the MS data were exported in netCDF format, and peak detection and alignment were performed using MetAlign software (Wageningen UR, The Netherlands). The resultant data were then exported in CSV format and analyzed using in-house analytical software. For semi-quantification, the peak height of each ion was calculated and normalized to the peak height of 2-isopropylmalic acid as an internal standard. Names were assigned to each metabolite peak based on the method described in a previous report [20].

### Statistical analysis

Data are expressed as median and range. Levels of serological markers and metabolites between the cohorts with and without cachexia were compared using the Mann-Whitney U test or Wilcoxon Signed-Rank test. Presence of intra-day variances in metabolite levels was then determined using Kruskal-Wallis multiple comparison (z-test) with bonferroni correction to compare values for each metabolite across all four time points assessed. Survival time was estimated using the Kaplan-Meier method. All statistical analyses were performed using NCSS 2007 software (NCSS, LLC. Kaysville, UT, USA).

## Results

### Patients' characteristics

From December 2009 to July 2011, 21 patients were enrolled in this study: 9 with cachexia and 12 without (Figure 1). Clinical characteristics are summarized in Table 1. Median body weight loss rates over 6 months in the cohorts with and without cachexia were 13.4% and 2.5%, respectively ($p = 0.0001$). Of the 21 patients enrolled, 19 had no history of prior treatment. No significant differences were noted in levels of tumor markers, LDH, CRP, or HbA1c between the cohorts. However, levels of total cholesterol and LDL cholesterol were significantly lower in the cohort with cachexia. Eight patients in the cohort with cachexia and 8 in that without were male in the present study. Median ages in the cohorts with and without cachexia were 66.5 (range, 36 to 77) and 68.5 (39 to 76) years, respectively ($p = 0.98$). No severe adverse events or unintended effects were noted among any participants in the present study.

**Table 1.** Patient characteristics.

| | | With Cachexia | Without Cachexia | p-value |
|---|---|---|---|---|
| | | n = 9 | n = 12 | |
| Age | (years) | 72 (39–76) | 64.5 (36–77) | 0.57 |
| Gender | Male/Female | 8/1 | 8/4 | 0.25 |
| PS | 0/1/2/3 | 0/5/3/1 | 4/8/0/0 | 0.005 |
| Stage | IVA/IVB | 5/4 | 5/7 | 0.54 |
| BW loss rate | (%) | 13.4 (10.2–30.8) | 2.5 (−5.2–4.6) | 0.0001 |
| Body weight | (kg) | 55.6 (45.0–77.0) | 57.5 (44.6–77.3) | 0.48 |
| Body mass index | | 22.6 (18.2–25.8) | 19.7 (16.5–26.1) | 0.15 |
| Anorexia | Gr 0/1/2/3 | 0/8/0/1 | 5/7/0/0 | 0.02 |
| Prior treatment | (No/Yes) | 8/1 | 11/1 | 0.83 |
| Laboratory data | | | | |
| WBC | (/μL) | 5100 (4100–17600) | 5850 (3000–111600) | 0.97 |
| Hb | (g/dL) | 11.9 (9.3–15.2) | 13.7 (11.3–14.6) | 0.20 |
| TP | (g/dL) | 6.4 (4.8–6.8) | 6.7 (6.0–7.5) | 0.15 |
| Alb | (g/dL) | 3.2 (2.1–4.7) | 3.9 (3.5–4.4) | 0.14 |
| LDH | (U/L) | 169 (125–228) | 179 (127–340) | 0.27 |
| TChol | (mg/dL) | 131 (99–167) | 187 (136–205) | 0.001 |
| LDL | (mg/dL) | 72 (45–91) | 100 (71–143) | 0.02 |
| HDL | (mg/dL) | 42 (22–73) | 53 (29–93) | 0.20 |
| TG | (mg/dL) | 90 (44–112) | 112 (62–159) | 0.09 |
| CRP | (mg/dL) | 1.9 (0.1–2.64) | 0.55 (0.1–6.97) | 0.89 |
| $HbA_{1c}$ | (%) | 5.7 (4.8–6.5) | 6.4 (4.6–7.3) | 0.11 |
| Tumor marker | | | | |
| CEA | (ng/mL) | 5.0 (1.4–29.2) | 4.7 (2.0–883.7) | 1.00 |
| CA19-9 | (U/mL) | 271 (5–1974) | 379 (1–80673) | 0.43 |
| DUPAN-2 | (U/mL) | 560 (33–230000) | 605 (25–140000) | 0.89 |

Abbreviations: PS, Eastern Cooperative Oncology Group performance status; BW loss rate, body weight loss rate over 6 months; TChol, total Cholesterol; LDL, low-density lipoprotein; HDL, high-density lipoprotein; TG, triglyceride; CRP, C-reactive protein.

doi:10.1371/journal.pone.0113259.t001

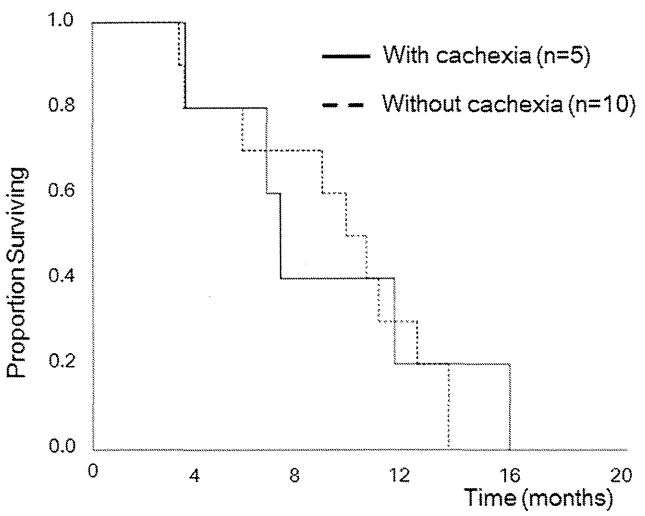


**Figure 2. Kaplan-Meier curve for overall survival in patients who had no prior treatment.**

doi:10.1371/journal.pone.0113259.g002

## Treatment and survival

After enrolling in this study, all 19 patients who had had no prior treatment subsequently received chemotherapy (n = 15) or chemoradiotherapy (n = 4). Regimens used in the 15 patients treated with chemotherapy were gemcitabine monotherapy (n = 13) and combination therapy of gemcitabine plus TS-1, an oral fluoropyrimidine prodrug (n = 2). In the four patients treated with chemoradiotherapy for locally advanced cancer, the regimens used (as part of another clinical study) were concurrent chemoradiotherapy with gemcitabine plus TS-1 (n = 2) and heavy-particle radiotherapy with gemcitabine (n = 2). The remaining 2 patients who had had prior treatment received best supportive care after enrolling in this study.

We analyzed survival in the 19 patients who had received no prior treatment. The median survival time in patients with stage IVA (n = 9) and stage IVB (n = 10) was 15.6 and 7.0 months (logrank test, $p<0.001$), respectively, while that in patients treated with chemotherapy (n = 15) and chemoradiotherapy (n = 4) was 9.5 and 19.7 months (logrank test, $p = 0.004$) respectively. Although this study was too small to detect survival difference, the median survival time in patients who received chemotherapy was 7.0 months with cachexia (n = 5) and 9.5 months without (n = 10) (logrank test, $p = 0.85$), and 1-year survival rates were 20.0% and 30.0%, respectively (Figure 2).

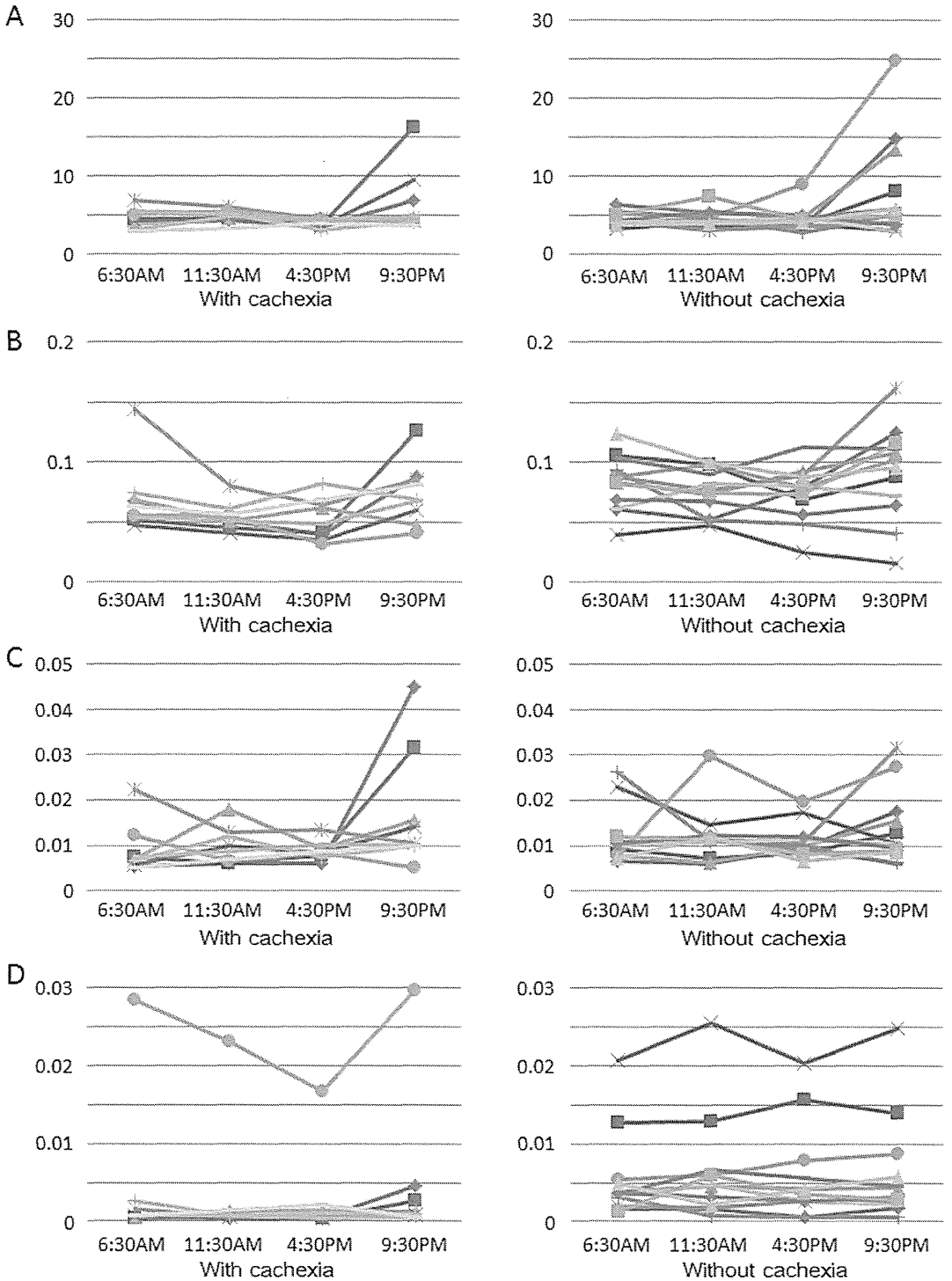


**Figure 3. Intra-day variation in A) lactic acid, B) alanine, C) catechol, and D) paraxanthine.**
doi:10.1371/journal.pone.0113259.g003

## Metabolomics

In our GC/MS-based metabolomics analysis system, which mainly targeted water-soluble metabolites, 124 metabolites were detected in subjects' serum samples (Table S1). Of these 124 metabolites, 1 metabolite, namely 2-isopropylmalic acid, was used as an internal standard, and 8 were probably extracted from non-serum source, for example from eppendorf tubes. These nine metabolites were therefore excluded from subsequent analyses.

Kruskal-Wallis multiple comparison (z-test) with bonferroni correction was used to evaluate changes in metabolite levels at four different time points throughout the day. These analyses showed that the levels of 60 of the 115 evaluated metabolites differed significantly between those means at any 1 of 4 time points. Univariate analysis of the 115 metabolites identified considerable inter-individual variability of levels of some metabolites throughout a single day. Figure 3 describes representative metabolites,